A Syd-1 homologue regulates pre- and postsynaptic maturation in *Drosophila*

David Owald,[1,2] Wernher Fouquet,[1,2] Manuela Schmidt,[3] Carolin Wichmann,[1] Sara Mertel,[1,2] Harald Depner,[1,2] Frauke Christiansen,[1,2] Christina Zube,[1] Christine Quentin,[1,2] Jorg Körner,[2] Henning Urlaub,[4] Karl Mechtler,[5] and Stephan J. Sigrist[1,2]

[1]Department of Genetics, Institute for Biology, Freie Universität Berlin, 14195 Berlin, Germany
[2]Bio-Imaging Center, Rudolf Virchow Center, 97078 Würzburg, Germany
[3]European Neuroscience Institute, 37077 Göttingen, Germany
[4]Max Planck Institute for Biophysical Chemistry, 37077 Göttingen, Germany
[5]Research Institute of Molecular Pathology, 1030 Vienna, Austria

Active zones (AZs) are presynaptic membrane domains mediating synaptic vesicle fusion opposite postsynaptic densities (PSDs). At the *Drosophila* neuromuscular junction, the ELKS family member Bruchpilot (BRP) is essential for dense body formation and functional maturation of AZs. Using a proteomics approach, we identified *Drosophila* Syd-1 (DSyd-1) as a BRP binding partner. In vivo imaging shows that DSyd-1 arrives early at nascent AZs together with DLiprin-α, and both proteins localize to the AZ edge as the AZ matures. Mutants in *dsyd-1* form smaller terminals with fewer release sites, and release less neurotransmitter. The remaining AZs are often large and misshapen, and ectopic, electron-dense accumulations of BRP form in boutons and axons. Furthermore, glutamate receptor content at PSDs increases because of excessive DGluRIIA accumulation. The AZ protein DSyd-1 is needed to properly localize DLiprin-α at AZs, and seems to control effective nucleation of newly forming AZs together with DLiprin-α. DSyd-1 also organizes trans-synaptic signaling to control maturation of PSD composition independently of DLiprin-α.

Introduction

Fast chemical synaptic transmission is mediated by precisely regulated neurotransmitter release from synaptic vesicles (SVs) at specialized presynaptic sites. This compartment, called the active zone (AZ), comprises a unique set of proteins (Schoch and Gundelfinger, 2006; Owald and Sigrist, 2009).

Genetic analyses of synapse assembly in *Caenorhabditis elegans* hermaphrodite-specific motor neuron synapses (HSNLs; Margeta et al., 2008) and in *Drosophila* neuromuscular junctions (NMJs; Collins and DiAntonio, 2007) have identified several presynaptic proteins important for AZ assembly (Owald and Sigrist, 2009). Syd-2/Liprin-α is needed for AZ formation at *C. elegans* HSNL synapses (Dai et al., 2006; Patel et al., 2006) and is important for proper AZ morphology in *Drosophila* (Kaufmann et al., 2002), and ELKS is essential downstream of Syd-2/Liprin-α (Dai et al., 2006). In *Drosophila*, the ELKS-related protein Bruchpilot (BRP) forms the electron-dense projection at AZs (T bar), and is crucial for AZ maturation (Kittel et al., 2006; Fouquet et al., 2009). Finally, Syd-1 (synapse defective 1), a multidomain RhoGAP-like protein, is required for *C. elegans* HSNL synapse assembly (Dai et al., 2006; Patel et al., 2006).

Here, a proteomics-based approach identified the *Drosophila* Syd-1 homologue (DSyd-1) as a BRP binding partner. Using stimulated emission depletion microscopy (STED; Kittel et al., 2006; Fouquet et al., 2009), we show that DSyd-1

D. Owald and W. Fouquet contributed equally to this paper.

Correspondence to Stephan J. Sigrist: stephan.sigrist@fu-berlin.de

M. Schmidt's present address is Dept. of Cell Biology, The Scripps Research Institute, La Jolla, CA 92037.

Abbreviations used in this paper: au, arbitrary units; ANOVA, analysis of variance; AZ, active zone; BRP, Bruchpilot; CNS, central nervous system; DVGlut, *Drosophila* vesicular glutamate transporter; eEJC, evoked excitatory junctional current; FA, formic acid; GluR, glutamate receptor; HSNL, hermaphrodite-specific motor neuron synapse; LC, liquid chromatography; MB, mushroom body; mEJC, miniature excitatory junctional current; MS, mass spectrometry; NGS, normal goat serum; NMJ, neuromuscular junction; PSD, postsynaptic density; STED, stimulated emission depletion microscopy; SV, synaptic vesicle; UAS, upstream activator sequence.

The Rockefeller University Press $30.00
J. Cell Biol. Vol. 188 No. 4 565–579
www.jcb.org/cgi/doi/10.1083/jcb.200908055

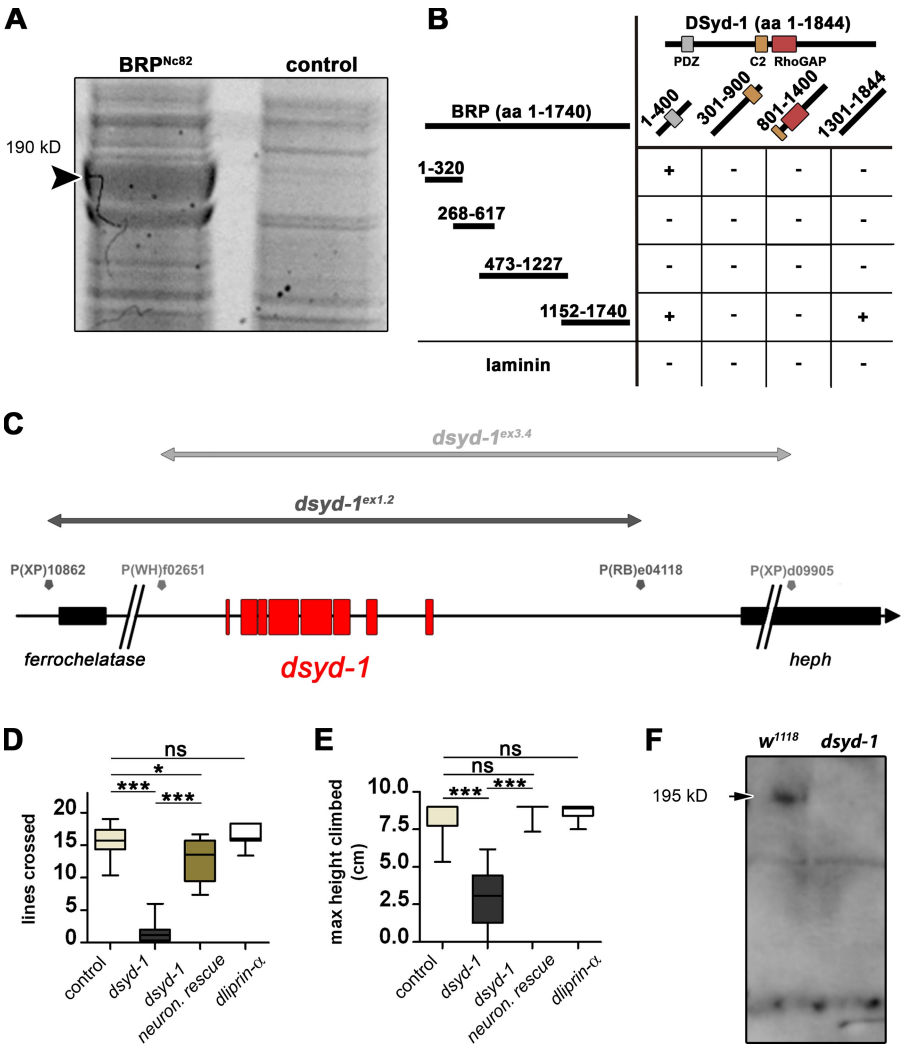

Figure 1. **Proteomics identify DSyd-1 as physical interactor of BRP.** (A) Monoclonal BRP^{Nc82} efficiently precipitates BRP (arrowhead), as seen in this SYPRO red–stained SDS-gel. Among other proteins, DSyd-1 was found to coprecipitate with BRP, as confirmed by MS/MS analysis. (B) Matrix showing yeast two-hybrid assay results confirming a direct physical interaction between BRP and DSyd-1. A C-terminal domain of BRP (aa 1,152–1,740) was positive for interaction with a C-terminal region of DSyd-1 (aa 1,301–1,844). Moreover, a bait N-terminal DSyd-1 (aa 1–400) fragment interacted with both the N-terminal fragment of BRP (aa 1–320) and a C-terminal BRP (aa 1,152–1,740) fragment. (C) Genomic location of *dsyd-1* on chromosome arm 3R at 100D2-100D3. *dsyd-1*–deficient animals were constructed using *Drosophila* lines carrying transposon-mediated flippase recognition target sites (Parks et al., 2004) that neighbored the *dsyd-1* locus (black, $dsyd\text{-}1^{ex1.2}$; gray, $dsyd\text{-}1^{ex3.4}$ in gray). We obtained two deficiencies that were confirmed with genomic PCR. In both cases, the entire *dsyd-1* locus (red) was excised, whereas in one case ($dsyd\text{-}1^{ex1.2}$, black line), the 5′ *ferrochelatase* was affected; and in the other case, the 3′ *heph* ($dsyd\text{-}1^{ex3.4}$, gray line) locus was affected. Taking these deficiencies in trans eliminates both copies of *dsyd-1*; however, this leaves one intact copy of each *heph* and *ferrochelatase*. (D and E) Behavioral tests demonstrate a requirement for DSyd-1 and less stringent requirement for DLiprin-α in the adult CNS. (D) Walking ability (control: 15.69 ± 0.57 lines, $n = 15$; *dsyd-1*: 1.62 ± 0.69 lines, $n = 8$; $dsyd\text{-}1^{rescue}$: 12.86 ± 0.99 lines, $n = 10$; *dliprin-α*: 16.19 ± 0.65 lines, $n = 7$; control × *dsyd-1*: $P = 0.0001$; control × $dsyd\text{-}1^{rescue}$: $P = 0.02$; control × *dliprin-α*: $P = 0.67$; *dsyd-1* × $dsyd\text{-}1^{rescue}$: $P < 0.0001$). (E) Negative geotaxis (control: 8.32 ± 0.37 cm; *dsyd-1*: 2.92 ± 0.60 cm; $dsyd\text{-}1^{rescue}$: 8.833 ± 0.17 cm; *dliprin-α*: 8.67 ± 0.15 cm; all: $n = 10$; control × *dsyd-1*: $P < 0.0001$; control × $dsyd\text{-}1^{rescue}$: $P = 0.32$; control × *dliprin-α*: $P = 0.91$; *dsyd-1* × $dsyd\text{-}1^{rescue}$: $P < 0.0001$). Impaired locomotive behavior in *dsyd-1* flies is rescued by pan-neural (*elav-GAL4*) reexpression of the *dsyd-1* cDNA. Error bars indicate the SEM. *, $P < 0.05$; ***, $P < 0.005$; ns, $P > 0.05$. (F) A polyclonal α-DSyd-1 antibody recognizes a band at the predicted molecular mass of 195 kD on immunoblots of w^{1118} control fly head lysate (arrow). This band is missing in *dsyd-1* head extracts. Statistics: Mann-Whitney test.

specifically localizes to a discrete compartment at the AZ edge, coordinating the BRP-composed T bar at the center of the AZ. Flies lacking DSyd-1 show impaired locomotion and a reduced life span, which is rescued by nervous system expression of the protein. Fewer release sites form at *dsyd-1* NMJs, and evoked neurotransmitter release is compromised, likely as a consequence of this. EM and STED results both show that *dsyd-1* mutant AZs often "overgrow" their T bars, and that ectopic electron-dense precipitates/BRP accumulations also form distant from AZs. Thus, DSyd-1 inhibits inappropriate localization of BRP and its associated electron density. Both DSyd-1 and DLiprin-α accumulate early during the protracted AZ formation process. Notably, DSyd-1 was needed to properly localize DLiprin-α at AZs, but not vice versa. Thus, one function of the RhoGAP DSyd-1 seems to be to stably target DLiprin-α to maturing AZs, allowing DLiprin-α to execute its AZ assembly function. Independent of DLiprin-α, the presynaptic AZ-localized protein DSyd-1 is also involved in defining the amount and composition of glutamate receptors (GluRs) accumulating at maturing postsynaptic densities (PSDs). DSyd-1 might stall synaptic proteins other than DLiprin-α, e.g., adhesion molecules, to regulate postsynaptic maturation in a trans-synaptic manner.

Results

The AZ protein BRP is an integral part of the electron-dense T bar and is needed for effective Ca^{2+} channel clustering during synapse maturation (Fouquet et al., 2009). Thus, BRP may be a platform for protein–protein interactions and was well-suited as a starting point for an unbiased proteomics screen for novel *Drosophila* AZ proteins.

Proteomic identification of *Drosophila* Syd-1 as a BRP-linked protein

Using the monoclonal antibody Nc82, we immunoprecipitated BRP from adult fly head extracts. Although BRP was strongly enriched in Nc82 precipitates, it was not detected in control eluates as visualized by staining SDS-polyacrylamide gels

(Fig. 1 A, arrowhead); this was confirmed by tandem mass spectrometry (MS/MS) using two independent protocols (see Materials and methods). Next, we subjected bands of coimmunoprecipitating proteins to MS/MS analysis. Several peptides (Fig. S1 A) were found to correspond to a conceptual protein annotated at FlyBase (http://flybase.org) as CG1976-PA or RhoGAP100F (for further identified proteins, see Fig. S1 B). Hereupon, we refer to this protein as DSyd-1 because of its striking similarity to *C. elegans* Syd-1, which has been implicated in AZ assembly (Hallam et al., 2002; Dai et al., 2006; Patel et al., 2006) and has been shown to physically interact with the BRP homologue ELKS (Patel and Shen, 2009). DSyd-1 is predicted to comprise a calcium-sensing/lipid-binding C2 domain, a PDZ protein–protein interaction domain, and a putative RhoGAP domain (Hallam et al., 2002).

To elucidate whether DSyd-1 can bind to BRP directly, subregions of each protein were tested for interaction in a yeast two-hybrid assay. Several interaction sites between both proteins were found (Fig. 1 B). We thus conclude that the physical interaction between Syd-1/DSyd-1 and ELKS/BRP is evolutionarily conserved.

Following the peptide sequence and an existing cDNA clone (Berkeley Drosophila Genome Project; available from GenBank/EMBL/DDBJ under accession no. LD28013; Fig. S1 A), a composite full-length cDNA was assembled, predicting a protein of 195 kD.

DSyd-1–deficient flies suffer from impaired locomotion and decreased lifespan

We generated *dsyd-1*–deficient animals using Flippase-mediated trans-deletion of flippase recognition target site–containing transposon lines (Parks et al., 2004) flanking the *dsyd-1* locus (Fig. 1 C). Two *dsyd-1*–deficient lines (*dsyd-1*$^{ex1.2}$ and *dsyd-1*$^{ex3.4}$) were isolated, and deletions were confirmed by genomic PCR (Parks et al., 2004). A combination of both chromosomes results in flies specifically deficient for *dsyd-1* (Fig. 1 C). Although *dsyd-1* adults appeared morphologically normal and, under optimal culturing conditions, eclosed close to the Mendelian ratio, they rarely survived longer than a week (>80% died within one week, n = 36). In contrast, >80% of control flies (n = 159) lived for at least two weeks. Moreover, the early lethality was completely overcome by *elav-GAL4*–driven pan-neuronal expression of the composite full-length cDNA (upstream activator sequence [UAS]–*dsyd-1*^{cDNA}) in the mutant background (n = 42). Notably, *dsyd-1* animals showed severely impaired locomotion, as revealed by two independent experimental settings, which was rescued by pan-neuronal expression of UAS–*dsyd-1*^{cDNA} as well (Fig. 1, D and E).

We raised a polyclonal antibody against a C-terminal peptide of DSyd-1 (DSyd-1 antibody) that identified a band of predicted size (195 kD) in adult head extracts and that was missing in extracts of *dsyd-1* mutants (Fig. 1 F).

DSyd-1 is an AZ protein

In situ hybridization showed nervous system–specific expression of *dsyd-1* (Fig. 2 A), with a similar onset of expression for *brp*, coincident with postmitotic differentiation (Wagh et al., 2006). The DSyd-1 antibody gave a neuropil-specific staining in larval (not depicted) and adult brains (Fig. 2 B), which was completely absent in *dsyd-1* mutant animals (Fig. 2 C) but restored upon pan-neuronal expression of UAS–*dsyd-1*^{cDNA} (not depicted). Co-labeling revealed a strong overlap with BRP^{Nc82} signals, which suggests that DSyd-1 is an AZ protein. To address this issue more explicitly, we first analyzed synapses within the mushroom body (MB) calyx. Here, postsynaptic specializations were labeled by expressing the GFP-labeled acetylcholine receptor subunit Dα7 within Kenyon cells (Fig. 2 D; Leiss et al., 2009; Raghu et al., 2009). DSyd-1–specific immuno-labeling was found to localize opposite to the Dα7 signal within the presynaptic terminals, which implies that DSyd-1 localizes to AZs (Fig. 2 D).

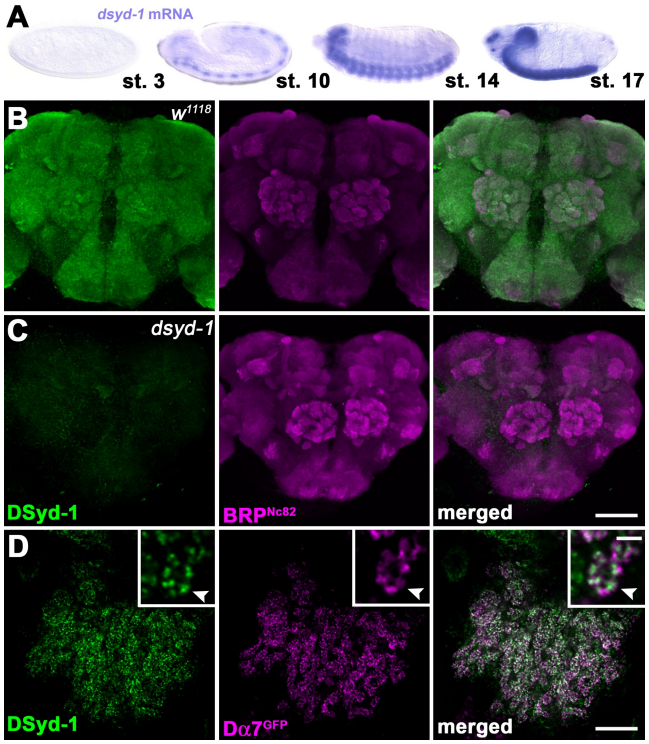

Figure 2. **DSyd-1 localizes to central synapses.** (A) In situ hybridizations show that *dsyd-1* is expressed throughout the embryo's CNS. st., stage. (B) Confocal z projection of adult *Drosophila* CNS. α-DSyd-1 staining co-localizes with BRP^{Nc82} throughout the brain, but is absent in *dsyd-1* animals (C). (D) DSyd-1 localizes opposite to postsynaptic acetylcholine receptors (Dα7^{GFP}) expressed in Kenyon cells at the adult MB calyx. Arrowheads in the inset panels (which show enlarged views) indicate pre- to postsynaptic alignment. Bars: (B and C) 50 µm; (D) 10 µm; (D, insets) 500 nm.

We then turned to the larval NMJ system (Fig. 3). Consistent with our observations in the MB calyx, the DSyd-1 antibody also specifically labeled AZs at NMJs (Fig. 3, A and B).

Both DSyd-1 and DLiprin-α localize at the AZ edge

Given that AZ assembly at HSNL synapses in *C. elegans* (Dai et al., 2006; Patel et al., 2006) involves a tight interplay between Syd-1 and Syd-2/Liprin-α, we reasoned that their homologues might operate together during synaptogenesis in flies. DLiprin-α is known to control proper segregation and shaping of AZs at the developing *Drosophila* NMJ (Kaufmann et al., 2002; Fouquet

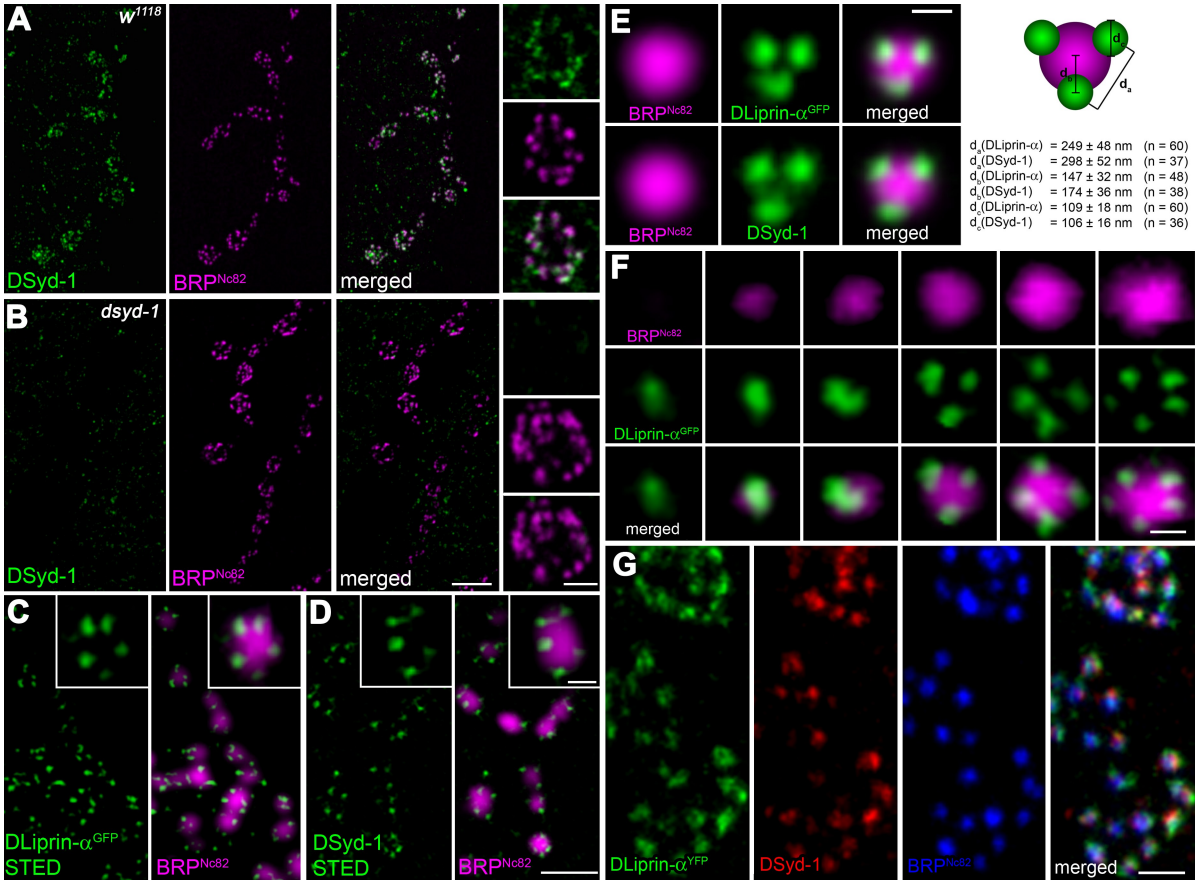

Figure 3. **DSyd-1 localizes to a subcompartment surrounding the AZ core.** (A) Boutons of larval NMJ innervating muscle 6/7. Most DSyd-1 clusters are found associated with BRP^{Nc82} signal, labeling AZs, as seen in high-magnification images (right). (B) There was no DSyd-1 staining at *dsyd-1*–deficient NMJs. (C) Single confocal slices of junctions expressing DLiprin-α^{GFP}, as described in Fouquet et al. (2009). STED images of α-GFP labelings show DLiprin-α^{GFP} as discrete spots arranged around the AZ core labeled by BRP^{Nc82}. (D) Single confocal slices of NMJs stained for endogenous DSyd-1 (STED) and BRP^{Nc82} (confocal). Distinct separable DSyd-1 spots closely resembling DLiprin-α distribution are arranged around the AZ center. (E) Merged images of several aligned planar imaged AZs of moderate size associated with three DLiprin-α or DSyd-1 clusters. The image shows BRP^{Nc82} in confocal resolution, α-GFP–labeled NMJs (for DLiprin-α^{GFP}), or DSyd-1–labeled NMJs imaged with STED. The arrangement of DSyd-1 clusters resembles that of the DLiprin-α clusters. d_a, distance between single clusters associated with the AZ; d_b, distance between AZ associated cluster and AZ center; d_c, diameter of clusters associated with AZs. (F) Single confocal slices of junctions expressing DLiprin-α^{GFP}. STED images of α-GFP show DLiprin-α^{GFP} as discrete dots arranged around the AZ core labeled by BRP^{Nc82}, ranging from one or two dots at small AZs to four or five dots at mature-sized AZs. (G) Triple labeling for DLiprin-α^{YFP}, DSyd-1, and BRP. Bars: (A and B) 2 µm; (A and B, insets) 500 nm; (C and D), 1 µm; (C and D, insets): 250 nm; (E) 250 nm; (F) 250 nm; (G) 500 nm.

et al., 2009). However, we noted that adults lacking DLiprin-α did not display the severe locomotor deficits seen in *dsyd-1* mutants, which suggests that both proteins may also have differentiated functions (Fig. 1, D and E).

Using STED microscopy, we recently showed that DLiprin-α forms discrete clusters surrounding the BRP-defined center of AZs (Fig. 3 C; Fouquet et al., 2009). We found DSyd-1 in clusters of similar size and distribution (Fig. 3, D and E) to DLiprin-α clusters. The number of DLiprin-α clusters varied according to the size of AZs (as judged by BRP immunoreactivity) ranging from one cluster at small AZs to four or five clusters at mature-sized AZs (Fig. 3 F).

Correlation analysis of DLiprin-α and DSyd-1 costainings (Fig. 3 G) indicated that both proteins closely colocalize ($R_{DSyd\text{-}1::DLiprin\text{-}\alpha} = 0.81 \pm 0.01$; $n = 12$), significantly closer than BRP and DLiprin-α ($R_{BRP::DLiprin\text{-}\alpha} = 0.66 \pm 0.01$; $P < 0.0001$, $n = 12$; Fig. 3 G). Moreover, the mean distances of individual DLiprin-α and DSyd-1 signals to neighboring spots or to the AZ core were comparable (Fig. 3 E). Thus, DSyd-1 and DLiprin-α together seem to define a common subcompartment surrounding the AZ core.

Reduction of evoked release at *dsyd-1* mutant NMJs

To explore whether DSyd-1 was needed for proper synaptic neurotransmitter release at AZs, two electrode voltage clamp recordings of late third-instar larval NMJs were performed. Evoked excitatory junctional currents (eEJCs) were significantly reduced in *dsyd-1* mutant larvae compared with controls (Fig. 4 A). These were significantly rescued by presynaptic expression of UAS–*dsyd-1*^{cDNA} using the motoneuronal driver *ok6-GAL4* (Fig. 4 A). For comparison, recordings from mutants in the AZ organizing protein *dliprin-α* were performed (compare Fig. 4 A with Kaufmann et al., 2002). Interestingly, eEJC amplitudes were decreased to a comparable level in *dsyd-1* and *dliprin-α*. Spontaneous miniature-current amplitudes, in turn, were on average not changed between *dsyd-1* and controls (Fig. 4 B, but see "Presynaptic DSyd-1 controls the amount…").

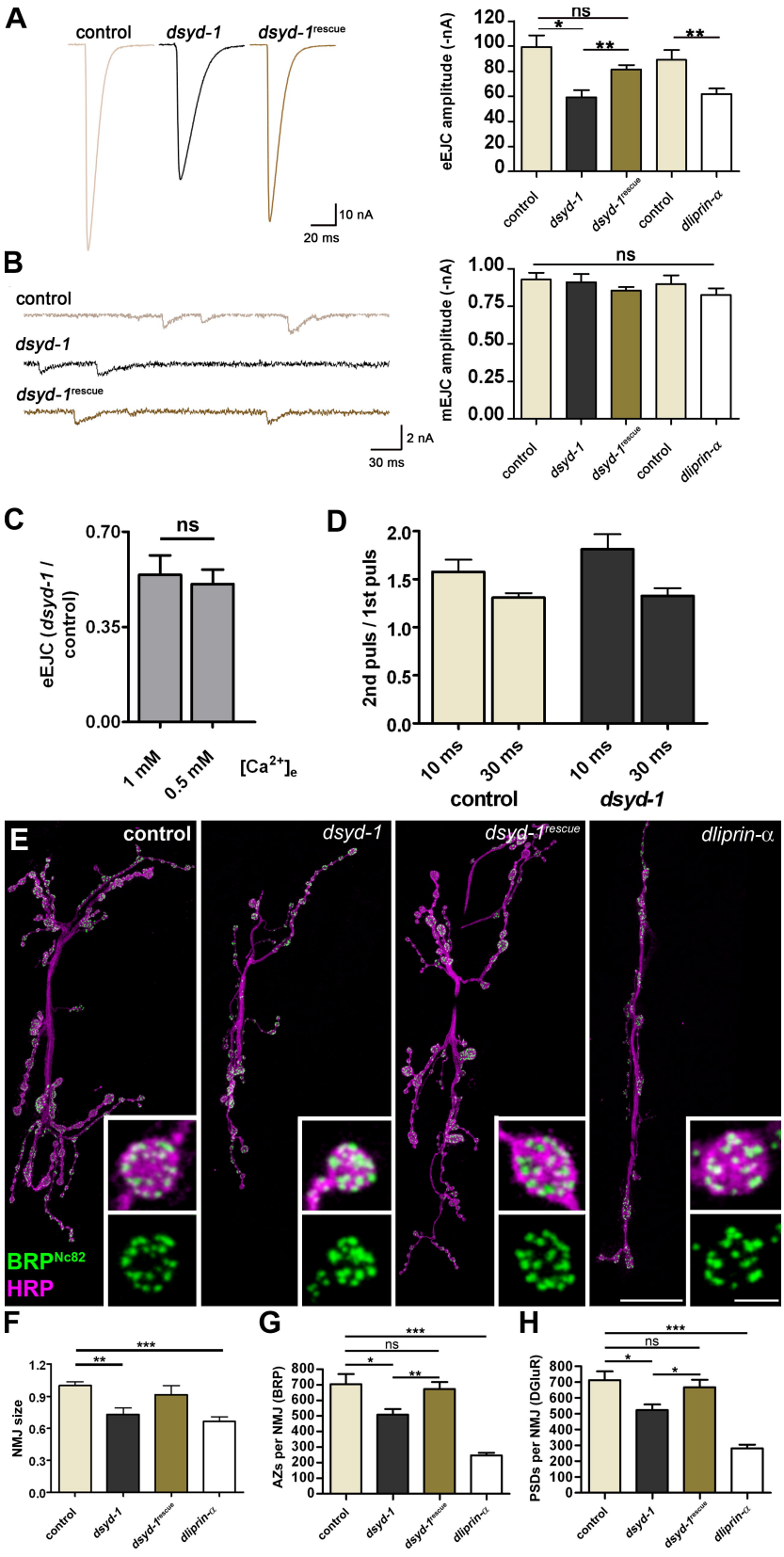

Figure 4. **Comparative analysis of NMJ morphology and function in *dsyd-1* and *dliprin-α* mutant animals.** (A) Mean traces (left) of eEJCs at 0.2-Hz nerve stimulation recorded from the larval NMJ at 1 mM extracellular calcium (muscle 6) for controls, *dsyd-1*, and *dsyd-1*^{rescue}; and mean eEJC amplitudes (right) for *dsyd-1* and control group (control: 99.3 ± 9.6 nA; *dsyd-1*: 59.2 ± 5.9 nA; both: $n = 9$, P = 0.01), *dsyd-1*^{rescue} (*dsyd-1*: 81.4 ± 4.5 nA, $n = 9$, P = 0.003; control: P = 0.162) as well as for *dliprin-α* and the control group (control: −89.4 ± 7.7 nA; *dliprin-α*: −62.0 ± 4.3 nA; both: $n = 7$, P = 0.007). Both *dliprin-α* and *dsyd-1* show reduced amplitudes compared with controls. This defect is significantly rescued by reexpressing *dsyd-1* cDNA in *dsyd-1*–deficient animals using a motoneuron-specific driver (*ok6-GAL4*). (B) Sample traces of mEJCs (right) for control, *dsyd-1*, and *dsyd-1*^{rescue} animals. Mean mEJC amplitudes (left) for controls (0.93 ± 0.05 nA, $n = 7$), *dsyd-1* (0.91 ± 0.05 nA, $n = 8$), and *dsyd-1*^{rescue} (0.86 ± 0.02 nA, $n = 9$), as well as *dliprin-α* (0.83 ± 0.05 nA, $n = 7$) and control (0.90 ± 0.06 nA, $n = 7$), are comparable (*dsyd-1* × control: P = 0.86; *dsyd-1* × *dsyd-1*^{rescue}: P = 0.54; control × *dsyd-1*^{rescue}: P = 0.14; control × *dliprin-α*: P = 0.46). (C) *dsyd-1* eEJC amplitudes normalized against mean control eEJC amplitude recorded at 1 mM (0.54 ± 0.07, $n = 11$) or 0.5 mM (0.51 ± 0.05, $n = 8$; P = 0.48) extracellular calcium, respectively. (D) Paired pulse experiments with a 10-ms (control: 1.58 ± 0.13, $n = 11$; *dsyd-1*: 1.81 ± 0.16, $n = 13$; P = 0.25) or 30-ms (control: 1.31 ± 0.05, $n = 12$; *dsyd-1*: 1.33 ± 0.08, $n = 12$; P = 0.98) interpulse interval recorded at 0.5 mM extracellular calcium. (E) Projection of confocal stacks of muscles 6 and 7 NMJs, labeled with antibodies recognizing BRP (BRP^{Nc82}, green) and HRP (magenta). Bars, 10 µm and 1 µm (insets). (F) Morphological size of *dliprin-α* and *dsyd-1* mutant NMJs was reduced compared with controls. The latter was rescued by motoneuron-specific reexpression of *dsyd-1*^{cDNA} (control: 1.0 ± 0.04, $n = 30$; *dsyd*-1: 0.73 ± 0.06, $n = 14$; *dsyd*-1^{rescue}: 0.91 ± 0.08, $n = 8$; *dliprin-α*: 0.66 ± 0.04, $n = 14$; control × *dsyd*-1: P < 0.01; control × *dsyd*-1^{rescue}: P > 0.05; control × *dliprin-α*: P < 0.001; *dsyd*-1 × *dsyd*-1^{rescue}: P > 0.05; *dsyd*-1 × *dliprin-α*: P > 0.05; *dsyd*-1^{rescue} × *dliprin-α*: P > 0.05, one-way analysis of variance [ANOVA]). (G) Number of AZs per NMJ counted via α-BRP^{Nc82} labeling. In both *dsyd-1* and *dliprin-α* mutants, AZ numbers were reduced compared with controls. The reduction seen in *dsyd-1* mutants was rescued by presynaptic *dsyd-1* cDNA expression (control: 704.6 ± 64.94, $n = 14$; *dsyd-1*: 508.6 ± 36.07, $n = 14$; *dsyd-1*^{rescue}: 673.1 ± 45.30, $n = 10$; *dliprin-α*: 247.3 ± 15.81, $n = 8$; control × *dsyd-1*: P = 0.020; control × *dsyd-1*^{rescue}: P = 0.75; control × *dliprin-α*: P = 0.0002; *dsyd-1* × *dsyd-1*^{rescue}: P = 0.008). (H) Number of PSDs defined by DGluRIID (not depicted). The results were comparable to those in G (control: 712.7 ± 55.24, $n = 20$; *dsyd-1*: 523.5 ± 36.35, $n = 13$; *dsyd-1*^{rescue}: 667.9 ± 46.85, $n = 8$; *dliprin-α*: 281.1 ± 22.83, $n = 7$; control × *dsyd-1*: P = 0.025; control × *C*: P = 0.86; control × *dliprin-α*: P = 0.0002; *dsyd-1* × *dsyd-1*^{rescue}: P = 0.047). Statistics: Mann-Whitney test. Error bars indicate the SEM. *, P < 0.05; **, P < 0.01; ***, P < 0.005; ns, P > 0.05.

Neurotransmitter release deficits at *dsyd-1* mutant NMJs might be explained by a drop in release probability of SVs, e.g., by a reduction of Ca^{2+} sensitivity of the SVs that are to be released. In this case, a change in short-term plasticity (paired pulse paradigm) or sensitivity to different extracellular Ca^{2+} concentrations should be observed. However, when we compared evoked release at two different Ca^{2+} concentrations, the ratio between *dsyd-1* mutant and control was unchanged (Fig. 4 C),

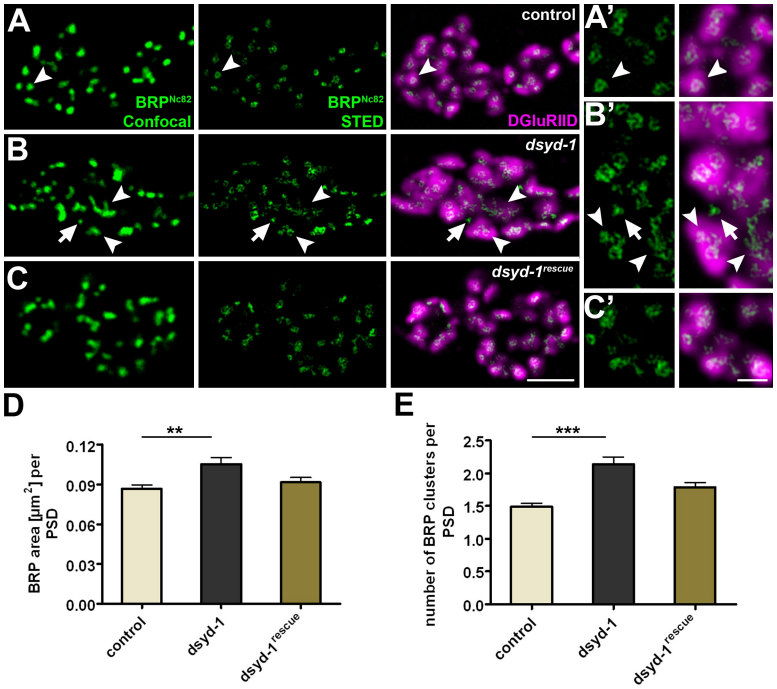

Figure 5. **Abnormal BRP clusters in *dsyd-1*.** (A–C) BRP puncta (confocal, left), BRP-donuts (STED, middle), and DGluRIID with BRP donuts (right). (A) The control BRP donut is indicated by arrowheads. (B) AZ size (arrowheads) is affected in *dsyd-1*. BRP donuts lacking postsynaptic DGluRIID receptors are observed as well (arrows). BRP donuts are frequently interconnected and abnormally shaped (arrowheads). (C) Defects are largely rescued by reexpression of UAS–*dsyd-1*^{cDNA}. Bar, 1 µm. (A′–C′) Magnified views of A–C. Bar, 250 nm. (D) Quantification shows elevated areas of individual BRP^{Nc82} clusters (control: 0.087 ± 0.002 µm^2, *n* = 298; *dsyd-1*: 0.105 ± 0.005 µm^2, *n* = 265; *dsyd-1*^{rescue}: 0.091 ± 0.004 µm^2, *n* = 207; control × *dsyd-1*: P < 0.01; control × *dsyd-1*^{rescue}: P > 0.05; *dsyd-1* × *dsyd-1*^{rescue}: P > 0.05). (E) Number of individual BRP clusters per single PSDs (control: 1.49 ± 0.05, *n* = 297; *dsyd-1*: 2.14 ± 0.12, *n* = 265; *dsyd-1*^{rescue}: 1.79 ± 0.08, *n* = 207; control × *dsyd-1*: P < 0.001; control × *dsyd-1*^{rescue}: P > 0.05; *dsyd-1* × *dsyd-1*^{rescue}: P > 0.05). Statistics: one-way ANOVA. Error bars indicate the SEM. **, P < 0.01; ***, P < 0.005.

which argues against a change in Ca^{2+} sensitivity. Moreover, no clear alteration in paired pulse behavior was observed (Fig. 4 D). Collectively, these data imply that the characteristics of SV release are (if anything) only moderately altered after loss of DSyd-1. Thus, the question arose as to the number of release sites (i.e., an individual PSD + adjunct AZ) forming at *dsyd-1* mutant NMJs, and/or whether the number of releasable SVs was reduced.

Reduced numbers of synaptic release sites at *dsyd-1* mutant NMJs

To account for SV numbers and distribution, we performed *Drosophila* vesicular glutamate transporter (DVGlut) immunostainings (Fig. S2 A; Daniels et al., 2004; Mahr and Aberle, 2006). Overall, both *dsyd-1* and control NMJs showed comparable immunoreactivity (Fig. S2 B), which indicates that the absolute number of SVs per terminal was not substantially changed. However, the SV signal appeared somewhat uneven between individual boutons at *dsyd-1* NMJs when compared with controls (Fig. S2 A). To evaluate whether this distribution would account for the observed release defect at low frequency stimulation (Fig. 4 A), SV distribution closely surrounding the electron-dense projection at AZs was evaluated in electron micrographs (Fig. S2, C and D). Here, the SV size (Fig. S2 E) as well as the number of SVs surrounding the AZs (Fig. S2, D and F) were comparable between control and *dsyd-1* mutant animals. We also tested whether mitochondria were properly transported to the NMJ terminal in *dsyd-1* mutants, using Mito^{GFP} (Fig. S2 G; Pilling et al., 2006). Here, the mean NMJ signal did not differ significantly between controls and mutants (Fig. S2 H).

To perform quantitative analysis of release sites, NMJs of third-instar larvae were stained (Fig. 4 E). The overall size of individual NMJs (as scored by HRP reactivity) was reduced in both *dliprin-α* and *dsyd-1* mutant animals (Fig. 4, E and F). We scored numbers of release sites by counting (a) BRP spots (for AZs, Fig. 4 E) and (b) DGluRIID spots (for PSDs, not depicted; Qin et al., 2005). In *dsyd-1* mutant larvae, a significant reduction of release sites was observed (Fig. 4, G and H). This reduction appeared identical when independently counting either BRP or DGluRIID spots, and was rescued by motoneuron-specific expression of UAS–*dsyd-1*^{cDNA} (Fig. 4, G and H).

Thus, presynaptic DSyd-1 is needed for developing NMJs to reach full morphological size and adopt a full complement of release sites. Consistent with previous studies, release site numbers were also reduced at *dliprin-α* mutant NMJs (Kaufmann et al., 2002); however, the phenotype is more pronounced than that observed in *dsyd-1* NMJs (Fig. 4, E, G, and H).

Defective AZ assembly and ectopic BRP accumulations at *dsyd-1* mutant terminals

Upon scoring BRP signals, we had the impression that atypically large spots formed at *dsyd-1* NMJs. To resolve AZ morphology more accurately, we used STED microscopy for the further analysis.

Using this technique, we recently showed that BRP is a direct building block of T bars. The N terminus of BRP localizes close to Ca^{2+} channels at the AZ membrane, whereas its C-terminus (recognized by the BRP^{Nc82}) defines the edge of the distal T bar platform, resulting in a typical donut-shaped appearance at wild-type NMJs (Fig. 5, A and A′, arrowheads; Fouquet et al., 2009).

At *dsyd-1* mutant AZs, this donut-type distribution was compromised (Fig. 5, B and B′, arrowheads) but was partially restored by UAS–*dsyd-1*^{cDNA} reexpression (Fig. 5, C and C′). In *dsyd-1*, BRP organization at individual sites often appeared enlarged (Fig. 5, B and B′, arrowheads; and Fig. 5 D)

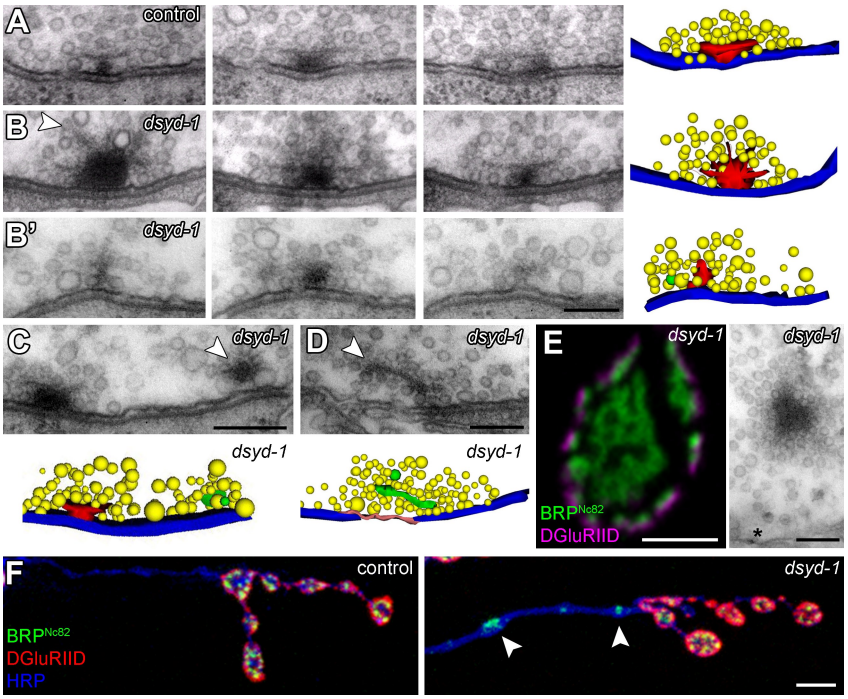

Figure 6. **Abnormal organization of T bars and floating electron-dense material in *dsyd-1* mutant animals.** (A–B′) Serial sections of misshapen T bars at *dsyd-1* (B and B′) AZs in comparison to control T bar (A). The arrowhead indicates filaments emerging from an overgrown T bar (B) in *dsyd-1*. (B′) Immature small T bar in *dsyd-1*. Reconstruction: red, T bar material; yellow, SVs; membrane blue, AZ. (C) Ectopic electron-dense material can be found at the edge of the AZ membrane (arrowhead, green in reconstruction); electron-dense material (arrowhead, green in reconstruction) associated with SVs is found proximal to AZs (D). (E) Ectopic BRP immunoreactivity (confocal image, left) and ectopic electron-dense material in the center of a *dsyd-1* mutant bouton (right). Ectopic electron-dense material (not depicted) and ectopic BRP immunoreactivity (F, arrowheads) are also found in axonal stretches. Bars: (A–B′) 100 nm; (C and D) 150 nm; (E, left) 1 µm; (E, right) 150 nm; (F) 1 µm.

and misshapen. Thus, the STED analysis implied that T bar morphology was affected, with atypical formation of large assemblies (Fig. 5, B and B′).

Individual synaptic release sites (as defined by presynaptic BRP in conjunction with opposing PSDs) showed further abnormalities. Although the size of individual PSDs was enlarged in *dsyd-1* mutants (see the following section), individual release sites (defined by the PSD) often comprised several BRP clusters (Fig. 5 E). Furthermore, spacing between individual AZs was irregular, and small BRP assemblies lacking adjacent GluR fields were observed (Fig. 5, B and B′, arrows). These might represent AZ assemblies, which do not progress to maturation properly due to a lack of nucleation assembly.

To address T bar morphology and the nature of increased BRP entities directly, we continued our studies using EM (Fig. 6 A) combined with 3D reconstruction of serial sections. In fact, at *dsyd-1* mutant NMJs (Fig. 6, B and B′), T bars often appeared irregular in shape, with pedestals of very high diameter and multiple, atypically prominent filamentous projections in their distal parts (Fig. 6 B, arrowhead). Such misshapen T bars (as in Fig. 6 B) were never observed in controls (Fig. 6 A). Moreover, atypically small T bar–like assemblies were apparent (Fig. 6 B′). These might reflect immature release sites and correspond to the small BRP assemblies observed by STED (Fig. 5, B and B′, arrows).

At control NMJs, electron-dense material is restricted to the T bar assembly at the center of the AZ (as defined by planar apposition between pre- and postsynaptic membrane). However, ectopic electron-dense material was easily observed at *dsyd-1* mutant NMJ terminals. Such material frequently appeared at the edge of AZs (Fig. 6 C), and was only loosely (Fig. 6 D, arrowhead), if at all (Fig. 6 E), associated with the presynaptic plasma membrane. Floating electron-dense material, highly decorated with SVs, was observed in the bouton interior (Fig. 6 E). As BRP seems to be a principal component of the electron-dense T bar (Fouquet et al., 2009), these ectopic electron-dense assemblies in *dsyd-1* mutants should contain BRP. Ectopic BRP reactivity at the bouton center and throughout the axon was also consistently detected by light microscopy (Fig. 6, E and F). In agreement with our EM data showing electron-dense material in association with SV-like material, ectopic axonal BRP accumulations colocalized with the SV marker DVGlut (Fig. S3; Daniels et al., 2004; Mahr and Aberle, 2006).

Collectively, fewer full-sized AZs formed in *dsyd-1* mutants, most likely because of the failure of some AZs to progress to maturation. However, excessive amounts of BRP were observed at the remaining AZs and within the neighboring plasma membrane and the presynaptic cytoplasm. Thus, DSyd-1 appears to be necessary to distribute AZ material adequately among a sufficient number of forming and maturing AZs. That the NMJ comprises a reduced number of immature AZs in *dsyd-1* mutants might contribute to the deposit of excess AZ material at remaining sites, effectively overgrowing them.

Presynaptic DSyd-1 controls the amount and composition of postsynaptic GluRs

At the *Drosophila* NMJ, ionotropic receptors (assembling as heteromeric tetramers by selecting four from five subunits) mediate the postsynaptic response to glutamate. Three subunits—DGluRIIC, IID, and IIE—are essential for receptor formation and function and are seemingly contained within all GluR complexes (Petersen et al., 1997; Marrus et al., 2004; Qin et al., 2005; Schmid et al., 2008). To assess PSDs in *dsyd-1* mutants, we looked into the distribution and signal intensity for different GluR subunits (Fig. 7, A–F).

When we stained *dsyd-1* mutants for DGluRIID, we recognized that individual GluR fields (reflecting individual PSDs) were dramatically enlarged at *dsyd-1* mutant NMJs

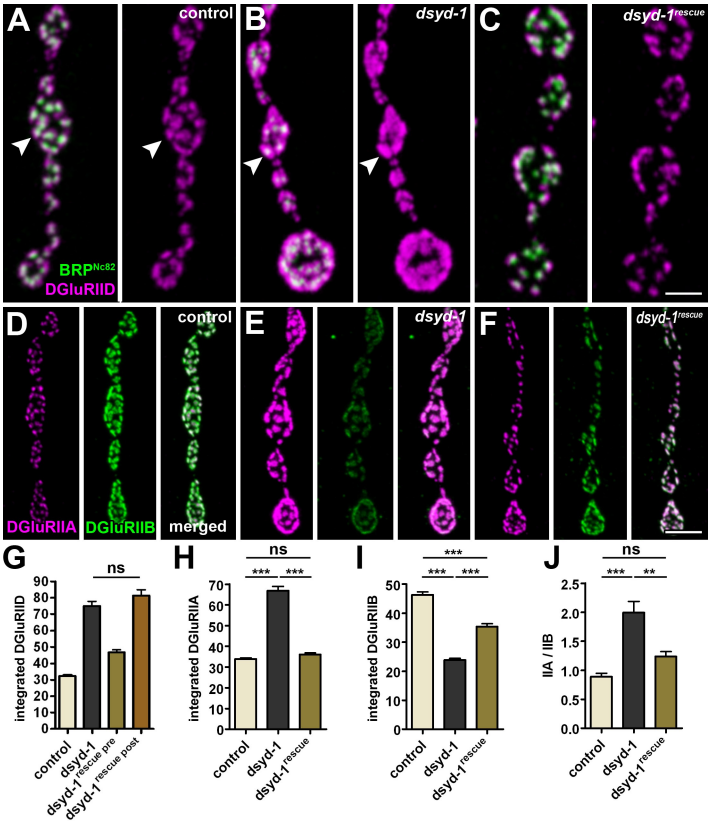

Figure 7. **DSyd-1 controls postsynaptic GluR field size and composition.** (A–C) Co-labeling of DGluRIID and BRP^{Nc82} for control (A), *dsyd-1* mutant (B), and presynaptically rescued (C) NMJs. Individual PSDs are indicated by arrowheads. (D–F) Co-labeling of DGluRIIA and DGluRIIB for control (D), *dsyd-1* mutant (E), and presynaptically rescued (F) NMJs. (G) Integrated DGluRIID signal (control: 32.25 ± 0.67 au, n = 1,314; *dsyd-1*: 74.86 ± 2.98 au, n = 335; *dsyd-1*$^{rescue\ pre}$: 46.71 ± 1.60 au, n = 515; *dsyd-1*$^{rescue\ post}$: 81.25 ± 3.54 au, n = 344; control × *dsyd-1*: P < 0.001; control × *dsyd-1*$^{rescue\ pre}$: P < 0.001; control × *dsyd-1*$^{rescue\ post}$: P < 0.001; *dsyd-1* × *dsyd-1*$^{rescue\ pre}$: P < 0.001; *dsyd-1* × *dsyd-1*$^{rescue\ post}$: P > 0.05; *dsyd-1*$^{rescue\ pre}$ × *dsyd-1*$^{rescue\ post}$: P < 0.001). (H) Integrated DGluRIIA signal (control: 33.88 ± 0.66 au, n = 1,064; *dsyd-1*: 66.85 ± 2.09 au, n = 667; *dsyd-1*^{rescue}: 36.31 ± 0.87 au, n = 830; control × *dsyd-1*: P < 0.001; control × *dsyd-1*^{rescue}: P > 0.05; *dsyd-1* × *dsyd-1*^{rescue}: P < 0.001). (I) Integrated DGluRIIB signal (E, control: 46.40 ± 0.99 au, n = 934; *dsyd-1*: 23.85 ± 0.60 au, n = 783; *dsyd-1*^{rescue}: 35.46 ± 0.89 au, n = 770; control × *dsyd-1*: P < 0.001; control × *dsyd-1*^{rescue}: P < 0.001; *dsyd-1* × *dsyd-1*^{rescue}: P < 0.001) size in *dsyd-1* mutants. (J) GluR field composition (control: 0.89 ± 0.06, n = 7; *dsyd-1*: 1.99 ± 0.19, n = 8; *dsyd-1*^{rescue}: 1.24 ± 0.08, n = 6; control × *dsyd-1*: P < 0.001; control × *dsyd-1*^{rescue}: P > 0.05; *dsyd-1* × *dsyd-1*^{rescue}: P < 0.01). Statistics: one-way ANOVA. Error bars indicate the SEM. **, P < 0.01; ***, P < 0.005; ns, P > 0.05. Bars: (A–C) 1 µm; (D–F) 2 µm.

(Fig. 5, A and B; and Fig. 7, A–C, arrowheads). This enlargement was rescued after presynaptic (using the motoneuron driver *ok6-GAL4*; Fig. 7, C and G) but not postsynaptic (using the muscle driver *G14-GAL4*; Fig. 7 G) expression of UAS–*dsyd-1*^{cDNA} (DSyd-1 failed to localize to PSDs when expressed in muscles; not depicted). Thus, presynaptic DSyd-1 has a role in defining the size of the postsynaptic GluR population. Each receptor also includes a fourth subunit, either DGluRIIA or DGluRIIB. These two GluR types differ in their single channel properties, and GluR composition also controls the morphological size of the NMJ and the number of individual synaptic contacts (DiAntonio, 2006). DGluRIIA levels were dramatically increased at *dsyd-1* mutant NMJs, but were restored to normal levels after presynaptic expression of UAS–*dsyd-1*^{cDNA} (Fig. 7, D–F and H). However, the levels of DGluRIIB were specifically reduced (Fig. 7, D–F and I), shifting the ratio between the two GluR types (Fig. 7 J).

As DGluRIIA complexes show higher single-channel conductance than DGluRIIB complexes (Schmid et al., 2008), one might expect enlarged miniature excitatory junctional currents (mEJCs) at *dsyd-1* NMJs. In Fig. 4 B, we show that mean mEJC amplitudes are not changed between *dsyd-1* mutants and controls. However, in histogram plots, a moderate tendency toward elevated frequencies of large mEJCs was observable for *dsyd-1* mutants (unpublished data). DGluRIIA-dominated NMJs also show slow decay kinetics (Schmid et al., 2008). Indeed, the mEJC decay τ recorded from *dsyd-1* mutant cells was increased by a mean of 12% compared with controls (n = 9 cells each, P = 0.006, Mann-Whitney test), whereas the eEJCs decay τ was ∼48% larger (n = 9 cells each, P = 0.008, Mann-Whitney test; compare with the traces in Fig. 4 A).

Collectively, parallel to its function of blocking overgrowth of presynaptic AZs, DSyd-1 has a specific function in restricting the size and defining the composition of postsynaptic GluR fields.

DLiprin-α is needed for the pre- but not the postsynaptic phenotype of *dsyd-1* mutants in embryos

Our behavioral analysis indicated that DSyd-1 shares functions with DLiprin-α, but that DSyd-1 also executes DLiprin-α–independent functions.

If both proteins solely acted in the same pathway, double mutant combinations should show similar phenotypes as single mutants. To test this, *dliprin-α; dsyd-1* double mutants were established. Although *dsyd-1* and *dliprin-α* single mutants survived to adulthood, double mutants were embryonic lethal, again indicating that the functions of both proteins do not fully overlap.

We asked whether the embryonic lethality of *dsyd-1; dliprin-α* might be due to an inability of the double mutant to form AZs and synapses altogether. Thus, ultrastructural analysis of high-pressure frozen/freeze-substituted (Fouquet et al., 2009) embryos was performed. T bars and planar synaptic membrane contacts were found in *dsyd-1* and *dliprin-α* single mutants, as well as in *dliprin-α*; *dsyd-1* double mutant embryos (Fig. 8 A). Hence, synapse formation including T bar assembly can in principle proceed in the absence of both proteins. We therefore consider DSyd-1 and DLiprin-α not to be structurally essential for AZ formation but rather to promote this process (Fig. 8 A).

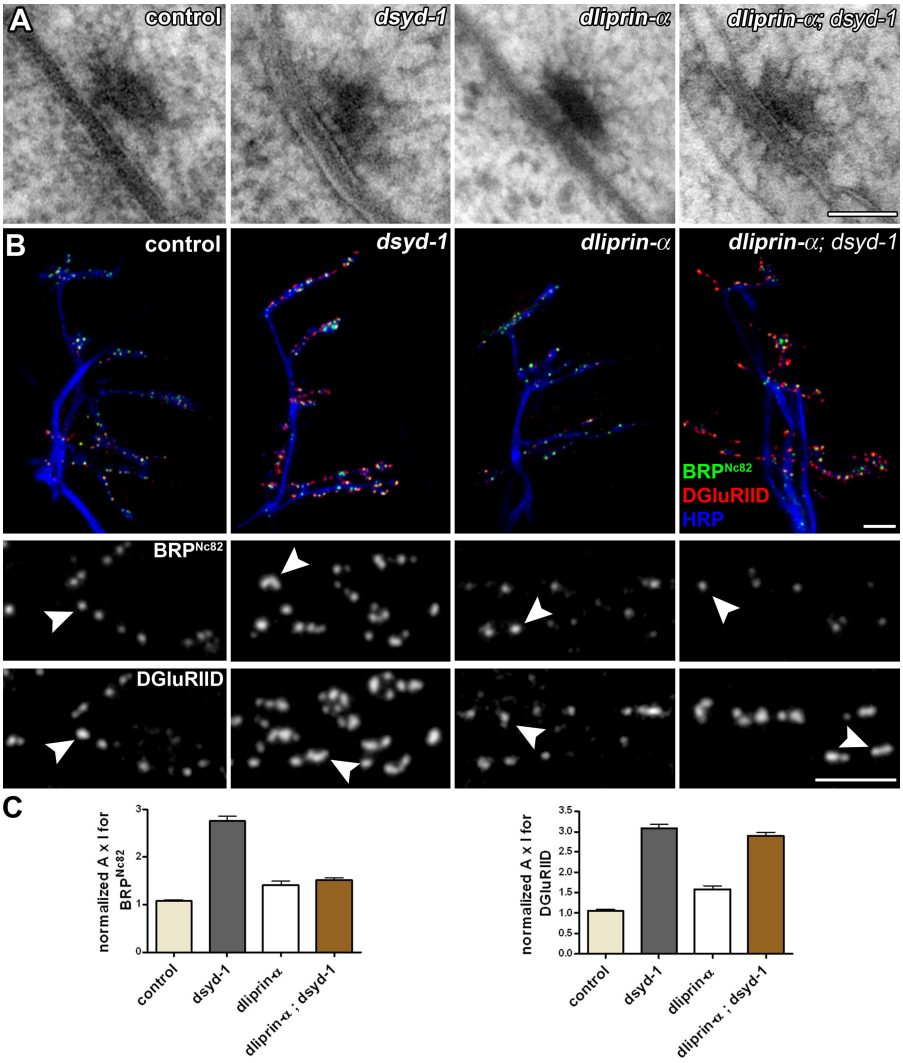

Figure 8. **Embryonic *dsyd-1* phenotypes.** (A) High-pressure freeze/freeze substitution–prepared NMJ synapse of control, *dsyd-1*, *dliprin-α*, and *dliprin-α; dsyd-1* double mutant embryos. All genotypes still form electron-dense projections (T bars) at the AZ. (B) Immunostaining of a region comprising muscles 6/7, 12/13, and 4 in late embryos of control, *dsyd-1*, *dliprin-α*, and *dliprin-α; dsyd-1*. Staining: HRP, BRP, and DGluRIID. (B, middle and bottom) Magnifications showing single synapses, with arrowheads denoting BRP (middle) and DGluRIID (bottom) puncta in the indicated mutants. (C) Quantification of BRP and DGluRIID signals at embryonic synapses. BRP signal in *dsyd-1* single mutants is significantly increased compared with control, *dliprin-α*, and *dliprin-α; dsyd-1* double mutants. DGluRIID is increased to a similar extent in *dsyd-1* and *dliprin-α; dsyd-1* double mutants compared with control and *dliprin-α* mutant animals. Statistics for BRP were as follows. Control: 1.07 ± 0.027, $n = 735$; *dsyd-1*: 2.75 ± 0.11, $n = 457$; *dliprin-α*: 1.41 ± 0.079, $n = 183$; *dliprin-α; dsyd-1*: 1.51 ± 0.054, $n = 446$; control × *dsyd-1*: $P < 0.001$; control × *dliprin-α*: $P < 0.05$; control × *dliprin-α; dsyd-1*: $P < 0.001$; *dsyd-1* × *dliprin-α*: $P < 0.001$; *dsyd-1* × *dliprin-α; dsyd-1*: $P < 0.001$; *dliprin-α* × *dliprin-α; dsyd-1*: $P > 0.05$. Statistics for DGluRIID were as follows. Control: 1.06 ± 0.029, $n = 765$; *dsyd-1*: 3.08 ± 0.10, $n = 541$; *dliprin-α*: 1.59 ± 0.080, $n = 218$; *dliprin-α; dsyd-1*: 2.90 ± 0.088, $n = 612$; control × *dsyd-1*: $P < 0.001$; control × *dliprin-α*: $P < 0.001$; control × *dliprin-α; dsyd-1*: $P < 0.001$; *dsyd-1* × *dliprin-α*: $P < 0.001$; *dsyd-1* × *dliprin-α; dsyd-1*: $P > 0.05$; *dliprin-α* × *dliprin-α*, *dsyd-1*: $P < 0.001$. Statistics: one-way ANOVA. Error bars indicate the SEM. Bars: (A) 70 nm; (B, top) 2 µm; (B, middle and bottom) 1 µm.

We further analyzed embryonic synapse morphology using BRP as a presynaptic marker and DGluRIID as a postsynaptic marker in single and double mutant combinations (Fig. 8, B and C). Compared with controls, BRP reactivity was clearly elevated at *dsyd-1*, but only very mildly at *dliprin-α* mutant NMJs (Fig. 8 B). Notably, BRP levels at *dliprin-α; dsyd-1* double mutant NMJs were comparable to those at *dliprin-α*, rather than to those at *dsyd-1* mutant NMJs (Fig. 8 B). Thus, loss of DSyd-1 leads to an increase in recruitment of BRP to AZs, which is dependent on the presence of DLiprin-α. Increased levels of BRP were also observed at *dsyd-1* mutant larval NMJs (Fig. 5).

Levels of DGluRIID were drastically increased at *dsyd-1* and equally at *dsyd-1*; *dliprin-α* double mutant NMJs, but only mildly elevated in *dliprin-α*–deficient synapses (Fig. 8, B and C). Thus, DSyd-1 is involved in regulating GluR field size, independently of DLiprin-α.

DSyd-1 is needed for proper AZ localization of DLiprin-α, but not vice versa

Using extended in vivo imaging of identified release sites, we recently showed that accumulation of DLiprin-α precedes accumulation of DGluRIIA as well as—by hours—the arrival of BRP throughout AZ assembly (Rasse et al., 2005; Schmid et al., 2008; Fouquet et al., 2009).

To place DSyd-1 into the temporal context of AZ assembly, we coexpressed ^{GFP}DSyd-1 (which, when pan-neuronally expressed, rescues the sluggish behavior of *dsyd-1* mutant adults) and BRP-short^{mStraw} in motoneurons. As expected from immunostainings (Figs. 2 and 3), presynaptic expression of DSyd-1 labeled AZs (Fig. 9, A and B). Individual NMJs were reimaged after 12 h, and substantial growth of the NMJ along with the addition of new AZs was observed (Fig. 9 A). DSyd-1 clearly and invariably preceded BRP at newly forming release sites (Fig. 9 A, arrowheads).

We went on to co-image DLiprin-α^{GFP} and ^{mStraw}DSyd-1. Newly formed AZs were usually decorated with both DLiprin-α^{GFP} and ^{mStraw}DSyd-1, suggesting that both proteins arrived at synaptic sites in very close temporal proximity (Fig. 9 B, arrows and arrowheads). Thus, newly forming AZs are characterized by DLiprin-α and DSyd-1–positive clusters from early on.

Genetic analysis in *C. elegans* has placed the putative RhoGAP DSyd-1 upstream of Syd-2/Liprin-α in the assembly hierarchy (Dai et al., 2006; Patel et al., 2006). We questioned whether both factors would reciprocally influence their distribution and AZ localization (Fig. 10, A–E). As expected

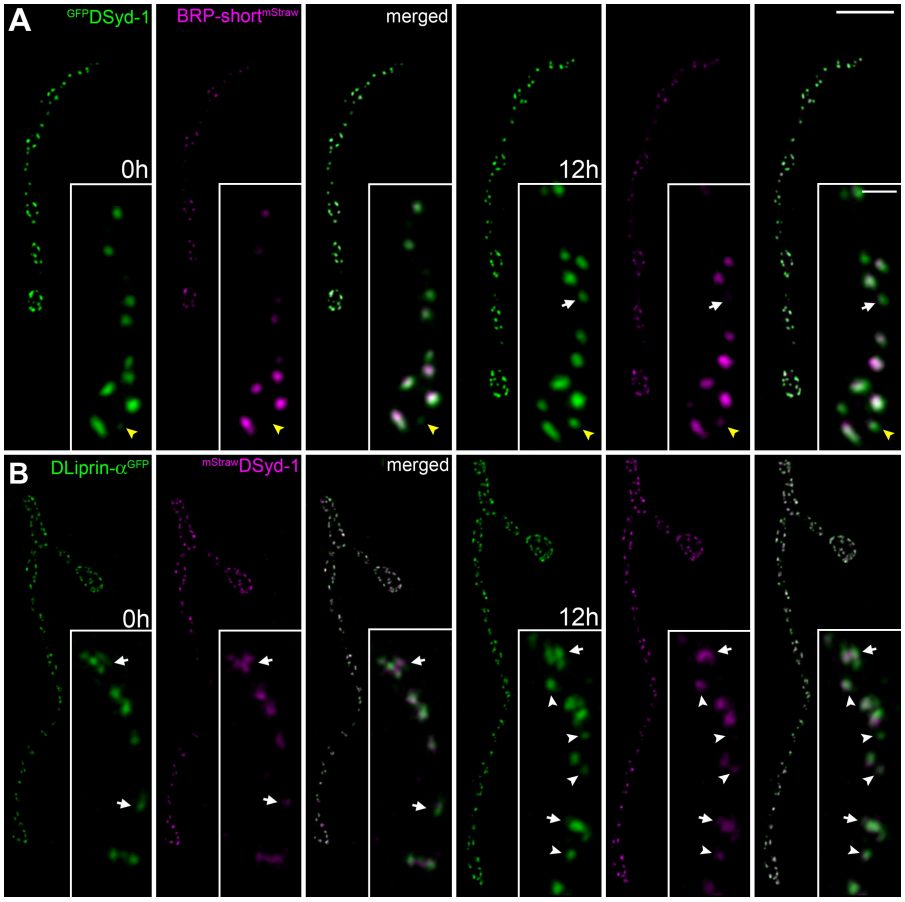

Figure 9. **DSyd-1 accumulates early during AZ assembly.** Confocal stacks of sequentially in vivo imaged NMJs (muscle 26), Δt = 12 h. NMJs coexpressing ^{GFP}DSyd-1 and BRP-short^{mStraw} (A), and DLiprin-α^{GFP} and ^{mStraw}DSyd-1 (B). (A) DSyd-1 preceded BRP (arrows and arrowheads) at 65% of the newly forming AZs, and BRP preceded DSyd-1 at 0%. The situation was not resolved at 35% (*n* = 37). (B) DLiprin-α and DSyd-1 accumulate in close temporal proximity (arrows and arrowheads): DLiprin-α preceded DSyd-1 at 26% of newly forming AZs, and DSyd-1 preceded DLiprin-α at 6%. The situation was not resolved at 68% (*n* = 35). Bars: (A and B) 4 µm; (A and B, insets) 500 nm.

(Fouquet et al., 2009), at control NMJs (Fig. 10 A), DLiprin-α and BRP colabeled individual AZs in a regular pattern (Fig. 10 A, arrowheads). Notably, DLiprin-α showed a highly irregular distribution at *dsyd-1* mutant terminals (Fig. 10 B), with many AZs (identified via BRP) lacking adequate DLiprin-α labeling (Fig. 10 B, arrowheads). Large DLiprin-α spots distant from BRP spots were often observed, which indicates the presence of ectopic accumulations of DLiprin-α (Fig. 10 B, arrows). After coexpression of DSyd-1 together with DLiprin-α at *dsyd-1* NMJs, however, most BRP-positive AZs showed DLiprin-α labeling (Fig. 10 C, arrowheads). In contrast, DSyd-1 targeted normally to AZs in *dliprin-α* mutants (compare Fig. 10 D with Fig. 10 E). Thus, presynaptic DSyd-1 is needed to properly localize DLiprin-α to AZs, but DLiprin-α is apparently not needed to target DSyd-1.

We also asked whether DSyd-1 would localize to *brp* mutant terminals. BRP arrives late during synapse assembly and is needed for proper maturation of release sites, as shown for the distribution of calcium channels (Fouquet et al., 2009). Although DSyd-1 targeted to AZs (Fig. 10 F), the distribution of the protein appeared somewhat "smeared," suggesting that BRP is needed for the proper spacing of DSyd-1 at mature AZs.

Discussion

Mechanisms which regulate assembly and maturation of presynaptic AZs are not well understood (Jin and Garner, 2008). We identified the *Drosophila* Syd-1 homologue (DSyd-1) as a binding partner of BRP. We found (Fig. 9; Fouquet et al., 2009) that DLiprin-α and DSyd-1 mark presynaptic sites where, subsequently, AZs (and adjunct PSDs) originate and mature, whereas BRP and Ca^{2+} channels accumulate at later time points than DLiprin-α and DSyd-1. DLiprin-α previously has been shown to be important for proper AZ formation (Kaufmann et al., 2002). Thus, consistent with reduced numbers of AZs forming at NMJs of *dsyd-1* and *dliprin-α* mutants (Fig. 4 G; and Kaufmann et al., 2002) and with both proteins being localized to AZs, the accumulation of DLiprin-α and DSyd-1 at nascent AZs may be instrumental for transforming selected sites into AZs, a process we refer to as "AZ nucleation activity." However, as the morphological size of *dsyd-1* NMJs is reduced, as is the AZ number (Fig. 4 F, G), in principle, other growth processes might also become rate-limiting at *dsyd-1* mutant NMJs. In other words, reduced AZ numbers could also be a consequence of a reduction in morphological NMJ growth. Studying the coupling between morphological growth and AZ formation will be important for determining the relevance of morphological size to total AZ number.

Work on en passant synapses of the *C. elegans* HSNL motor neuron implies that, in genetic terms, Syd-1 operates upstream of Syd-2/Liprin-α. This is based on the fact that a Syd-2/Liprin-α dominant allele can bypass the requirement of *syd-1* (Dai et al., 2006), which indicates that the protein's essential role in AZ assembly at HSNL synapses is mediated via Syd-2/Liprin-α.

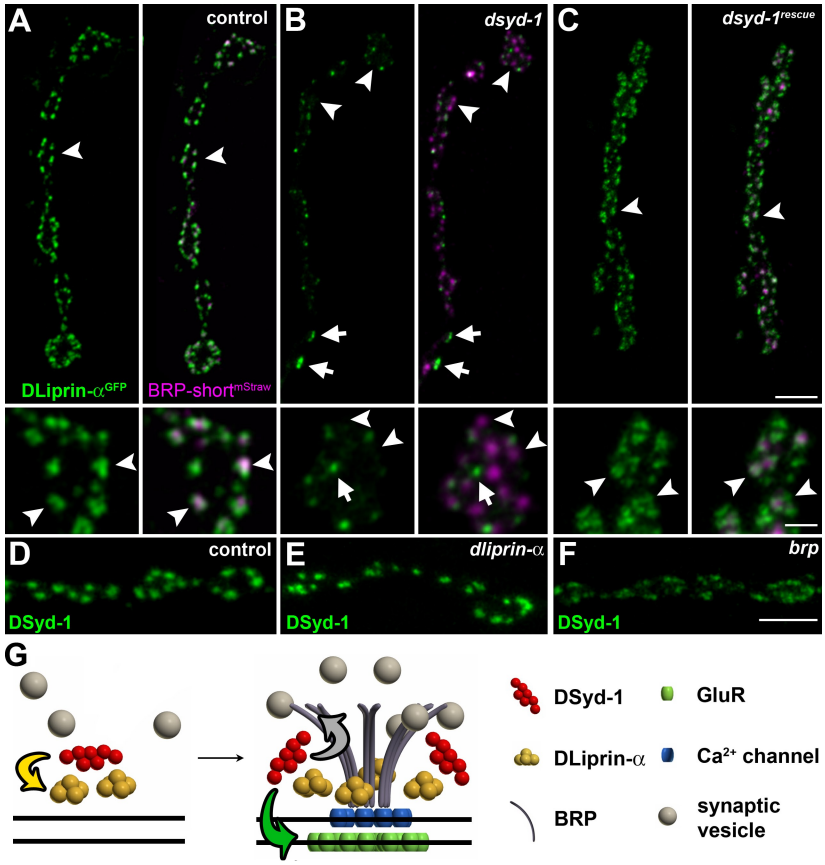

Figure 10. **Defective DLiprin-α localization in *dsyd-1* mutants.** (A–C) DLiprin-α^{GFP}/BRP-short^{mStraw} co-imaging in control (A), *dsyd-1* (B), and *dsyd-1^{rescue}* (C) are shown. The localization of DLiprin-α is changed at *dsyd-1* mutant NMJs, but is rescued by reexpression of UAS–*dsyd-1^{cDNA}* in motoneurons. Bars, 2 µm and 500 nm (insets). Arrowheads indicate AZs marked by BRP and arrows indicate ectopic DLiprin-α in *dsyd-1* mutants. (D–F) DSyd-1 localizes to AZs in control (D), *dliprin-α* (E), and *brp* (F) animals. (G) Model of AZ assembly. Yellow arrow, DSyd-1 regulates DLiprin-α early in assembly; green arrow, DSyd-1 regulates GluR field size; gray arrow, DSyd-1 binds BRP and regulates BRP supply. Bars: (A, top): 2 µm; (A, bottom) 500 nm; (F) 2 µm.

We here provide evidence that DSyd-1 is required to properly target DLiprin-α to AZs. In the absence of DSyd-1, DLiprin-α distributes unevenly at NMJ terminals, sparing many AZs. Thus, we provide direct evidence that the RhoGAP DSyd-1 operates upstream in AZ assembly in vivo: DSyd-1 seemingly stalls DLiprin-α to developing AZs in order to allow for the AZ nucleation function of DLiprin-α to effectively operate.

DLiprin-α seems to be a direct substrate of DSyd-1 (Fig. 10 G). Our data imply that other presynaptic substrate proteins of DSyd-1 might exist at nascent synapses, a finding that is unexpected based on analysis of AZ formation in *C. elegans*. Therefore, we deduce from our findings that presynaptic DSyd-1 (but apparently not DLiprin-α) plays an important role in shaping the PSD assembly. Embryos and larvae mutants for *dsyd-1*, and importantly, *dliprin-α; dsyd-1* double mutant embryos (the double mutant is embryonic lethal), showed increased overall amounts of postsynaptic GluRs, whereas *dliprin-α* single mutant embryos (Fig. 8) and larvae did not (not depicted). These increased amounts of GluRs in *dsyd-1* mutants vanished after presynaptic reexpression of UAS–*dsyd-1^{cDNA}*. It is tempting to speculate that the presynaptic DSyd-1 protein helps the AZ localization of an adhesion protein, which via trans-synaptic interaction might steer the incorporation of postsynaptic GluRs (for a model, see Fig. 10 G). A potential role of the Neurexin–Neuroligin axis should be evaluated in this context (Li et al., 2007; Südhof, 2008).

Drosophila NMJs express two functionally distinct GluR complexes, DGluRIIA and IIB, which influence the number of release sites formed (DiAntonio, 2006). Individual PSDs form distinctly from preexisting ones, and mature over hours, switching from DGluRIIA to IIB incorporation throughout maturation in a manner dependant on presynaptic signaling (Rasse et al., 2005; Schmid et al., 2008). DSyd-1 might mediate such a maturation signal, as *dsyd-1* mutants show excessive amounts of DGluRIIA incorporation at PSDs. This regulation is likely not (or only partially) due to compensation for reduced presynaptic glutamate release, as *dliprin-α* mutants (with similarly reduced transmission levels) do not show this dramatic increase in GluR levels.

Despite enlarged receptor fields and specifically elevated DGluRIIA levels, average miniature event amplitudes were comparable between *dsyd-1* animals and controls, which we currently cannot account for. A possible explanation might comprise regulatory processes rendering populations of receptors non-/partially functional. Nonetheless, EJC decay time constants of dsyd-1 mutants resemble those found at *dgluRIIB*-deficient (and thus GluRIIA dominated) NMJs (Schmid et al., 2008).

Which processes are downstream of the DSyd-1–mediated DLiprin-α activity at nascent AZs? Liprin family proteins steer transport in axons and dendrites (e.g., of AMPA receptors) to support synaptic specializations (Wyszynski et al., 2002; Shin et al., 2003; Wagner et al., 2009). Notably, *in dsyd-1* mutants, although many AZs lacked proper amounts of DLiprin-α, large ectopic accumulations of DLiprin-α were observed. At the same time, ectopic accumulations of BRP/electron density were observed in the absence of DSyd-1. It is tempting to

speculate that these ectopic pools of DLiprin-α provoke the aberrant accumulation of electron densities in *dsyd-1* mutants, which is consistent with the transport function of DLiprin-α (Miller et al., 2005) and the direct interaction of DLiprin-α/Syd-2 and ELKS/BRP (Patel and Shen, 2009). Consistently, large BRP accumulations observed in *dsyd-1* embryos were no longer present in *dsyd-1*; *dliprin-α* double mutants, which indicates that the presence of DLiprin-α is needed to provoke these overaccumulations of BRP when DSyd-1 is missing.

In the absence of DSyd-1, BRP was inappropriately localized, even within the cytoplasm, forming ectopic electron-dense material (which is consistent with its role as building block for the electron-dense T bars). Such "precipitates" also occurred at and close to non-AZ membranes. Moreover, at *dsyd-1* AZs, large malformed T bars formed. Thus, it appears plausible that DSyd-1 keeps BRP "in solution" to organize its proper consumption at AZs. An alternate and not mutually exclusive explanation may be that axonal BRP precipitates also reflect defects in axonal transport due to the absence of DSyd-1. The presence of several binding interfaces between BRP and DSyd-1 may be considered as a basis for regulating their interplay.

BRP accumulation in the center of the AZ is also in the center of the functional and structural AZ assembly process (Kittel et al., 2006; Wagh et al., 2006; Fouquet et al., 2009). It appears likely that BRP assembly is regulated on multiple levels. Notably, although BRP accumulation is severely compromised in mutants for the kinesin *imac* (Pack-Chung et al., 2007), it is not fully eliminated. Moreover, the serine/arginine protein kinase SRPK79D was recently shown to associate with BRP and to repress premature "precipitation" of BRP in the axons (Johnson et al., 2009; Nieratschker et al., 2009). Furthermore, mutants for the serine/threonine kinase *unc51* have recently been shown to suffer from BRP targeting defects (Wairkar et al., 2009). Phosphorylation of DSyd-1 (e.g., within serine-rich stretches toward the C terminus) might be involved in regulating proper longer-range transport ("blocking precipitation on the way") as well as proper delivery of BRP at nascent AZ sites.

Recently, the Rab3 GTPase has been shown to be crucial for effective nucleation of BRP at AZs (Graf et al., 2009). In an interesting parallel to *dsyd-1* defects, *rab3* mutant NMJs showed fewer BRP-positive AZs; however, if present, BRP levels were increased. Nonetheless, instead of overgrown T bars, as observed in *dsyd-1* mutants, *rab3* mutants rather showed multiple T bar AZs (Graf et al., 2009). It will be interesting to investigate whether these pathways act in parallel or converge, along with their relationships to other synaptogenic signals (Giagtzoglou et al., 2009; Owald and Sigrist, 2009).

Materials and methods

Proteomics

Protein extraction protocols were modified from Luo et al. (1997). Wild-type adult fly heads were mechanically homogenized in deoxycholate buffer (500 mM Tris, pH 9.0, and 1% sodium-deoxycholate containing protease inhibitor cocktail [Roche]) followed by incubation at 36°C for 30 min. 0.1% Triton X-100 was added thereafter, and the lysate was incubated at 4°C for 30 min. After centrifugation for 15 min at 16,000 *g*, the supernatant was used in immunoprecipitations with the monoclonal antibody BRP^{Nc82} (provided by E. Buchner, Universität Würzburg, Würzburg, Germany) or mouse IgG heavy chain (for control; Dianova) cross-linked to protein A–Sepharose (Bio-Rad Laboratories). After incubation at 4°C for 2 h, beads were washed in deoxycholate/Triton X-100 buffer. In a first approach, proteins were removed en masse from the BRP^{Nc82}–Protein A beads with 100 mM glycine, pH 2.0, reduced with dithiothreitol, carboxymethylated using iodoacetamide, and digested with trypsin (Betschinger et al., 2003). Peptides were extracted with formic acid (FA) and separated by nano–high-performance liquid chromatography (LC) on a PepMap C18 reversed-phase column. Eluting peptides were transferred online to an ion trap mass spectrometer (LTQ; Thermo-Fisher Scientific).

In a second approach, proteins were eluted from the MAB Nc82–Protein A beads with SDS sample buffer. The samples were separated by one-dimensional SDS-PAGE (NuPAGE 4–12% gradient gel; Invitrogen), and protein bands were visualized using SYPRO red (Invitrogen). The elution and control lanes (controls, i.e., immunoprecipitation with mouse IgG) were each cut in 2-mm-thick stripes so that the regions of both lanes aligned with each other.

Each individual stripe was digested in gel with trypsin (sequencing grade; Roche), and peptides were extracted according to Shevchenko et al. (1996). Dried samples from in-gel digests were dissolved in 10% (vol/vol) acetonitrile (CH_3CN; LiChrosolve grade; Merck & Co., Inc.), and 0.15% FA (Sigma-Aldrich). The sample volumes were adjusted to the sample amount. The dissolved samples were subjected to a nano-LC coupled electrospray ionization tandem MS using an orthogonal quadruple time-of-flight mass spectrometer (Q-Tof Ultima; Waters). The nano-LC system was equipped with a C18 pepMap100 column (75 µm ID, 3 µm, 100 Å; Dianex) running with a flow rate of 180 nl/min. The buffers used were as follows: buffer A (H_2O and 0.1% [vol/vol] FA) and buffer B (80% [vol/vol] acetonitrile and 0.1% [vol/vol] FA). The gradient applied was 90% (vol/vol) buffer A to 55% (vol/vol) buffer A in 60 min, 55% (vol/vol) buffer A to 10% (vol/vol) buffer A in 5 min, and 5 min with 10% (vol/vol) buffer A. Before separation of the peptides by nano-LC, samples were desalted with online coupled precolumns (3 mm) consisting of the same chromatography material. The electrospray was generated with fused-silica 10-µm PicoTip needles (New Objective, Inc.) and was operated at ~1.8–2.3 kV. Fragment spectra of sequenced peptides were searched against all entries of the nonredundant Database from the National Center for Biotechnology Information using the software search algorithms MASCOT (Matrix Science Ltd.). For the database search, no constraints on molecular weight or biological species were applied.

Both approaches identified DSyd-1 in BRP^{Nc82} immunoprecipitates as physical interactors of BRP; however, DSyd-1 was not detected in control immunoprecipitations.

Yeast two-hybrid

dsyd1 constructs were obtained by PCR on pUASt/*dsyd 1* (see the Molecular cloning paragraph) and cloned into pGAD-T7 and pGBK-T7 (both from Takara Bio Inc.). *brp* constructs have been described previously (Fouquet et al., 2009). In principle, all experiments were conducted as described previously (Fouquet et al., 2009). All cotransformation experiments were conducted according to the yeast two-hybrid protocols of Takara Bio Inc., using the strain AH109. In brief: to ensure the presence of both cotransformed plasmids, the yeast was plated on minimal synthetic defined (SD)/−Leu/−Trp medium plates. After growing for 2–3 d, at least 10 clones each were analyzed on SD/−Ade/−His/−Leu/−Trp/X-α-gal medium plates to select for positive interaction. If >90% of the clones grew (and turned blue in color), this was regarded as positive interaction. As a positive control, pGBKT7-p53 was cotransformed with pGADT7 containing the SV40 large T antigen. Negative controls consisted either of laminin as bait together with the prey to be tested or the corresponding bait together with the empty prey vector (Fouquet et al., 2009).

Genetics

Fly strains were reared under standard laboratory conditions (Sigrist et al., 2003). Either w^1 or w^{1118} strains were used as background for generation of transgenes (BestGene, Inc.). *dsyd-1* mutants (*dsyd-1*$^{ex3.4}$, eliminating the complete *dsyd-1* and partially deleting the 3′ *heph* locus; and *dsyd-1*$^{ex1.2}$, eliminating the complete *dsyd-1* locus and partially deleting the 5′ *ferrochelatase* locus) were constructed and validated by genomic PCR according to Parks et al. (2004). For *dliprin-α*, *dliprin-α*^{EPexR60}/*dliprin-α*^{F3ex15} (Kaufmann et al., 2002) was used. *dliprin-α*^{EPexR60}; *dsyd-1*$^{ex3.4}$ and *dliprin-α*^{F3ex15}; *dsyd-1*$^{ex1.2}$ were kept using the T(2;3)CyOGFP-TM3GFP compound balancer (Eissenberg et al., 2005).

Genotypes used for in vivo imaging were (all from a w^- background): (a) *ok6-GAL4*, UAS-BRP-short^{mStraw}/+; UAS–^{GFP}DSyd-1/+; (b) *ok6-GAL4*, UAS–^{GFP}DLiprin-α /+; UAS–^{mStraw}DSyd-1/+; (c) UAS-Mito^{GFP}/*ok6-GAL4*

and UAS-Mito^{GFP}/*ok6-GAL4*; *dsyd-1*$^{ex1.2}$/ *dsyd-1*$^{ex3.4}$; (d) UAS–^{GFP}DLiprin-α, UAS-BRP-short^{mStraw}/*ok6-GAL4*; (e) UAS–^{GFP}DLiprin-α, UAS-BRP-short^{mStraw}/*ok6-GAL4*; *dsyd-1*$^{ex1.2}$/*dsyd-1*$^{ex3.4}$; (f) UAS–^{GFP}DLiprin-α, UAS-BRP-short^{mStraw}/*ok6-GAL4*; *dsyd-1*$^{ex1.2}$, UAS–DSyd-1/*dsyd-1*$^{ex3.4}$; (g) *dliprin-α*^{F3ex15}/*dliprin-α*^{EPexR60}; *D42-GAL4*/ UAS–^{GFP}DSyd-1; and (h) *brp*^{69}/DfBSC29, *ok6-GAL4*; UAS–^{GFP}DSyd-1/+.

Genotypes used for DLiprin-α immunostainings were: *ok6-GAL4*/+; UAS–DLiprin-α^{GFP}/+ and *ok6-GAL4*, UAS–DLiprin-α^{YFP}/+ (van Roessel et al., 2004). For DSyd-1 immunostainings in the MB calyx, UAS–Dα7^{EGFP}/+; *ok107-GAL4*/+ was used.

Antibody and Western blotting

A rabbit serum against C-terminal SSGDSKNGSDEYDDIK was produced (Eurogentec). Serum was affinity purified with the same peptide. *Drosophila* fly head extracts (five heads per lane) were probed with affinity-purified antibody (dilution of 1:500).

In situ hybridization

Whole-mount embryonic in situ hybridizations were performed essentially as described by the Berkeley Drosophila Genome Project (http://www.fruitfly.org/). For the *dsyd-1* sense RNA probe (Berkeley Drosophila Genome Project; available from GenBank/EMBL/DDBJ under accession no. LD28013) was cut with XhoI and in vitro transcribed using T7 RNA polymerase. For antisense probes, LD28013 was cut with EcoRI, and SP6 RNA was in vitro transcribed.

Molecular cloning

As the partial clone (GenBank accession no. LD28013) was available, a full-length *dsyd1* cDNA was designed according to the exon prediction of FlyBase. For this, the bps 1,183–2,933 not covered by LD28013 were amplified by elongase PCR from adult fly head cDNA using 5′-CCAGTGGGTCCCTCGAGAAGAATG-3′ and 5′-TCCAAATCAGCGCCGAAGAGC-3′. The resulting fragment was StuI digested and ligated with LD28013. This ligation was digested with XhoI, ligated into pBluescript KS (+) (Agilent Technologies), cut out with XhoI–XbaI, and ligated into pUASt (pUASt/*dsyd-1*, bps 1,183–*5,537*). Bps 1–1,182 were amplified by elongation of PCR from fly head genomic DNA using 5′-ATGACGGTGCAACCGGCTGAAATG-3′ and 5′-CGTTGACATTCTTCTCGAGGGA-3′. Fragments without introns were amplified via vent PCR. A: (A1) 5′-GAGCGCGGCCGCGATGACG-3′ and (A2) 5′-GAACTGATCTTCCATTTTCCGCCATTTCAGCCGGTTGCAC-3′; B: (B1) 5′-TGCAACCGGCTGAAATGGCGGAAAATGGAAGATCAG-3′ and (B2) 5′-CCGCAAGGATTTCGTCGCCCACCCGCAAGCAGCCG-3′; C: (C1) 5′-CAACAGCGGCTGCTTGCGGGTGGGCGACGAAATCCT-3′ and (C2) 5′-CCGTCATTTCGCGACCATCTCGTGATGAGCGCGGCCTC-3′; and D: (D1) 5′-CCGAGGCCGCGCTCATCACGAGATGGTCGCGAAATGAC-3′ and (D2) 5′-TCCCGTTGACATTCTTCTCG-3′). Fragments A and B were linked via elongation PCR using A1 and B2, and fragments C and D were linked using primers C1 and D2. The resulting fragments were linked using primers A1 and D2. Bps 1–1,182 and pENTER were digested with NotI and XhoI, and ligated. Bps 1,183–*5,537* were amplified via PCR from pUASt/*dsyd-1* bps 1,183–*5,537* using the primers 5′-GTCCGCCAGTGGGTC-3′ and 5′-GTCTATTCTAGACTTGATGTCATCGTACTCAT-3′. pENTER/*dsyd-1* (Wagh et al., 2006) bps 1–1,182 and *dsyd-1* bps 1,183–*5,537* were digested with XhoI and XbaI, and ligated thereafter. All sequences were validated by double strand sequencing. pUASt/*dsyd-1* cDNA and pTGW/*dsyd-1*^{cDNA} constructs were obtained using the Gateway system (Invitrogen).

Image acquisition

Image acquisition of confocal microscopy was obtained with a confocal microscope (TCS SP5; Leica). STED microscopy was performed with a TCS STED microscope (Leica). Images of fixed and live samples were acquired at room temperature. Confocal imaging of NMJs and whole brains was done using a z step of 0.5 µm. The following objectives were used: 20× 0.7 NA oil immersion for brain scans, 63× 1.4 NA oil immersion for NMJ and calyx confocal imaging, and a 100× 1.4 NA oil immersion STED objective for STED imaging (all from Leica). All images were acquired using the LCS AF software (Leica). For previous descriptions see Fouquet et al. (2009).

Immunostainings of larval and embryonic NMJs

Dissections were performed in HL3 by opening the larvae/embryo dorsally along the midline and removing the innards to grant visual access to the body wall muscles. Dissections were fixated with 4% paraformaldehyde in PBS (pH 7.2) for 10 min. After fixation, the filets were washed with PBS with 0.05% Triton-X 100 (PBT) and blocked for 30 min in 5% normal goat serum (NGS). For the immunostainings, the larvae were incubated with primary antibodies at 4°C overnight and subsequently washed in a 0.05% PBT solution for 12 h at room temperature. For the α-DSyd-1 stainings, the primary antibody was diluted in 0.3% PBT instead of 0.05%. Larvae were then incubated overnight with secondary antibodies at 4°C. Washing procedures were repeated. Immunocytochemistry was equal for both conventional confocal and STED microscopy. Larvae were finally mounted either in Vectashield (Vector Laboratories) or Mowiol (see also Qin et al., 2005). Antibody dilutions were: 1:100–1:200 M-α-Nc82 (provided by E. Buchner); 1:500 Rb-α-DSyd-1 ; 1:500 Rb-α-DGluRIID; 1:100 M-α-DGluRIIA (Developmental Studies Hybridoma Bank); 1:1,000 Rb-α-DGluRIIB (provided by D.E. Featherstone, University of Illinois at Chicago, Chicago, IL; Marrus et al., 2004; Liebl et al., 2005); 1:500 M-α-GFP (Invitrogen); 1:500 Rb-α-GFP (Invitrogen); 1:500 Rb-α-DVGlut (Hermann Aberle, Universität Münster, Münster, Germany); and HRP-Cy5 1:250 (Dianova). All confocal secondary antibodies were diluted 1:500. Secondary antibodies used for STED images (Sheep-α-M-Atto647N and Sheep-α-Rb-Atto647N; Sigma-Aldrich) were diluted 1:100.

Embryos were staged temporally (22–24 h) and morphologically, and stained as described for larvae.

Adult central nervous system (CNS) stainings

Brain stainings were essentially performed as described previously (Wu and Luo, 2006). Brains were dissected in HL3 on ice and immediately fixed in cold 4% PBS for 20 min at RT. The brains were then washed in 0.3% PBT (4× for 15 min) and preincubated in PBT with 10% NGS for 1 h at RT. For primary antibody treatment, samples were incubated in PBT containing 5% NGS and the primary antibodies for 2 d at 4°C. After primary antibody incubation, brains were washed in PBT for 4× for 20 min at RT, then overnight at 4°C. All samples were then incubated in PBT with 5% NGS containing the secondary antibodies (1:500) for 3 d at 4°C. Brains were finally washed for 4× for 20 min at RT, then stored overnight at 4°C, and transferred in Vectashield onto slides (Vector Laboratories).

Live imaging

Intact living *Drosophila* larvae were covered with Voltalef H10S oil (Arkema, Inc.) and placed into an airtight imaging chamber. During image acquisition, the larvae were shortly (10 to 20 min) anaesthetized by introducing a desflurane (Baxter) air mixture into the imaging chamber. Selected NMJs were exclusively located in abdominal segments A2 and A3 on muscles 26 and 27.

Also see Rasse et al. (2005) and Schmid et al. (2008). During incubation time, the imaged larvae were maintained at 25°C, which corresponded to our normal rearing temperature.

Image processing

Confocal imaging. Confocal stacks were processed with ImageJ software (http://rsbweb.nih.gov/ij/). Deconvolutions were used for single slices and confocal stacks. The ImageJ plug-ins used were iterative deconvolution and iterative deconvolution 3D, respectively (OptiNav, Inc.).

STED imaging. STED images were processed using linear deconvolution software integrated into the Imspector Software bundle (Max Planck Innovation GmbH). For visualization, images for figures were enhanced using the brightness/contrast function of ImageJ and edited in Photoshop (Adobe).

Quantifications of AZ/PSD number, size, and intensity

All images for synapse quantification from fixed samples were acquired using the same microscope settings. Control and mutant dissections were stained in the same vial.

To measure the number of synapses per NMJ, first, the original stack was scaled up twofold. A Gaussian filter with a radius of two pixels was applied. The contrast of the maximum projection of an image stack was adjusted in such way that the intensity maximum of the picture was set to 255 (min/max contrast function in ImageJ). Afterward, a threshold was set excluding all pixels with a value <51. The segmentation of single synapses was done by hand with the pencil tool and a line thickness of 2 pixels. The processed picture was then transformed into a binary picture; all pixels with a value <51 received the value "0" and all pixels with a value ≥51 were reassigned to a value of "255." This binary mask was then projected onto the original unmodified image using the "min" operation from the ImageJ image calculator. The synapses of the resulting images were counted with the help of the "analyze particle" function with the threshold set to 1.

The STED images were quantified using ImageJ. BRP^{Nc82} size quantification was performed as described in proceeding paragraph, whereas

the "analyze particles" tool was applied within a predefined region of interest surrounding single PSDs. The sum of the area of all BRP^{Nc82} particles was measured for each PSD, and the number of particles was subsequently counted. No Gaussian blur was applied here.

To define the DVGlut and $Mito^{GFP}$ signal intensity of NMJs, a region of interest was applied by surrounding the 1b innervations (based on the HRP signal), and the mean pixel intensity was measured. To compare several experiments, the mean signal was subsequently normalized to the corresponding HRP signal.

To compare different time points in live imaging experiments, all images were normalized by adjusting the brightest pixel composing the NMJ to 255 arbitrary units (au).

Two-electrode voltage clamp recordings

Two-electrode voltage clamp recordings were essentially performed as described by Fouquet et al. (2009). In brief: for *dsyd-1* (*ok6-GAL4/+; dsyd-1*), *dsyd-1* rescue (*ok6-GAL4/+; dsyd-1*, UAS–*dsyd-1*^{cDNA}*/dsyd-1*), and controls (w^{1118} *; ok6-GAL4/+*), as well as *dliprin-α* and controls (w^{1118}), recordings were made from late third-instar larvae (muscle 6, segments A2 and A3; experimental groups consisted of either males or females only). For all experiments, the recording solution consisted of HL3: 70 mM NaCl, 5 mM KCl, 20 mM $MgCl_2$, 10 mM $NaHCO_3$, 5 mM trehalose, 115 mM sucrose, 5 mM Hepes, and 1 or 0.5 mM $CaCl_2$, pH adjusted to 7.2. The cells from which recordings were made had an input resistance ≥ 4 MΩ. Intracellular electrodes were filled with 3 M KCl, and resistances ranged from 10 to 25 MΩ. Stimulation artifacts of eEJCs were removed for clarity. Paired pulse stimulation protocols and analyses were essentially performed as in Kittel et al. (2006). Paired pulse intervals were either 10 ms or 30 ms, and experiments were performed in 0.5 mM extracellular calcium. For determination of the base line of the second pulse at the 10-ms interpulse interval, the decay of the first pulse was extrapolated.

Transmission EM

For high-pressure freezing, ∼2–10 (22–24 h) staged *Drosophila* embryos were placed in aluminum specimen carrier 200 µm deep (type A; Leica), filled with yeast paste, and covered with a lid (specimen carrier type). The samples were frozen immediately in a high-pressure freezing machine (HPM010; Bal-Tec) and rapidly transferred to liquid nitrogen for storage.

Freeze substitution and embedding were performed in acetone in a freeze-substitution device (EM AFS; Leica). In brief, freeze substitution was performed in acetone with 0.1% tannic acid at –90°C for 4 d, followed by acetone with 2% osmium during the last 7 h. The samples were warmed (5°C/h) to –20°C and incubated for 16 additional hours before being warmed (10°C/h) to 4°C. At 4°C, the samples were washed in acetone and warmed to room temperature. They were then embedded in epon (see Rostaing et al., 2006; Siksou et al., 2007).

Subsequently, 55–65-nm (gray-silver) sections were cut using an ultramicrotome (EM Ultracut 6; Leica). Sections were collected on formvar-coated 100-mesh grids. Sections were dried and post-stained with uranyl acetate and lead citrate as described previously (Schmid et al., 2006). Micrographs were taken with a 1024 × 1024 charge-coupled device (CCD) detector (Proscan CCD HSS 512/1024; Proscan Electronic Systems GmbH) in a transmission EM (EM 902A; Carl Zeiss, Inc.) operated in bright field mode.

Conventional RT embedding was essentially performed as described previously (Wagh et al., 2006). Images were obtained from dissected preparations of third-instar larvae (NMJ 6/7, segments A2/A3). Instead of 1 h of fixation in 1% osmium tetroxide, the fixation was performed in 1% osmium tetroxide and 0.8% KFeCn in 0.1 M cacodylate buffer. After infiltration in epon resin, muscles were cut out (six animals for each genotype) and embedded in a single block.

Quantifications

The number of vesicles at the AZ was evaluated within three shells (each shell was 50-nm thick) surrounding the T bar (*n* w^1 = 26; *n dsyd-1* = 26 AZs). For the vesicle diameter, all vesicles in a radius of 150 nm surrounding the T bar were taken and the diameter was measured with the ImageJ software.

Reconstructions. For 3D-reconstructions of larval T bars (w^1 vs. *dsyd-1*), 3–5 serial 60-nm sections were reconstructed with the free software Reconstruct (Fiala, 2005).

Behavioral analysis

Female animals were tested within 48 h after eclosure and at least one night at 18°C. Before testing, flies were anesthetized on ice and wings were clipped. Experiments were performed under a red light, and animals were allowed to adapt to darkness for at least 1 h before testing. To test walking ability, flies were placed on a flat surface with a 2 × 2-cm grid and allowed to walk freely for 10 s. The number of lines crossed was counted. Negative geotaxis was measured with flies placed on the bottom of an empty, scaled food vial, and the maximum height (max = 9 cm) reached within 30 s was recorded.

Statistics

Data were analyzed with Prism (GraphPad Software). Asterisks are used to denote significance (*, $P < 0.05$; **, $P < 0.01$; ***, $P < 0.005$; ns, $P > 0.05$).

Online supplemental material

Fig. S1 shows the amino acid sequence of DSyd-1 with peptides identified via MS highlighted in red. Fig. S2 deals with the distribution of SVs and mitochondria in *dsyd-1* mutants. Fig. S3 shows that axonal BRP and DVGlut colocalize. Online supplemental material is available at http://www.jcb.org/cgi/content/full/jcb.200908055/DC1.

We would like to thank Franziska Zehe for excellent technical assistance and Ulrich Thomas for comments on the manuscript.

This work was supported by grants from the Deutsche Forschungsgemeinschaft to S.J. Sigrist (Exc 257, SI849/2-1 and 2-2, TP A16/SFB 551, TP B23/SFB581).

Submitted: 11 August 2009
Accepted: 21 January 2010

References

Betschinger, J., K. Mechtler, and J.A. Knoblich. 2003. The Par complex directs asymmetric cell division by phosphorylating the cytoskeletal protein Lgl. *Nature.* 422:326–330. doi:10.1038/nature01486

Collins, C.A., and A. DiAntonio. 2007. Synaptic development: insights from *Drosophila*. *Curr. Opin. Neurobiol.* 17:35–42. doi:10.1016/j.conb.2007.01.001

Dai, Y., H. Taru, S.L. Deken, B. Grill, B. Ackley, M.L. Nonet, and Y. Jin. 2006. SYD-2 Liprin-alpha organizes presynaptic active zone formation through ELKS. *Nat. Neurosci.* 9:1479–1487. doi:10.1038/nn1808

Daniels, R.W., C.A. Collins, M.V. Gelfand, J. Dant, E.S. Brooks, D.E. Krantz, and A. DiAntonio. 2004. Increased expression of the *Drosophila* vesicular glutamate transporter leads to excess glutamate release and a compensatory decrease in quantal content. *J. Neurosci.* 24:10466–10474. doi:10.1523/JNEUROSCI.3001-04.2004

DiAntonio, A. 2006. Glutamate receptors at the *Drosophila* neuromuscular junction. *Int. Rev. Neurobiol.* 75:165–179. doi:10.1016/S0074-7742(06)75008-5

Eissenberg, J.C., M. Wong, and J.C. Chrivia. 2005. Human SRCAP and *Drosophila melanogaster* DOM are homologs that function in the notch signaling pathway. *Mol. Cell. Biol.* 25:6559–6569. doi:10.1128/MCB.25.15.6559-6569.2005

Fiala, J.C. 2005. Reconstruct: a free editor for serial section microscopy. *J. Microsc.* 218:52–61. doi:10.1111/j.1365-2818.2005.01466.x

Fouquet, W., D. Owald, C. Wichmann, S. Mertel, H. Depner, M. Dyba, S. Hallermann, R.J. Kittel, S. Eimer, and S.J. Sigrist. 2009. Maturation of active zone assembly by *Drosophila* Bruchpilot. *J. Cell Biol.* 186:129–145.

Giagtzoglou, N., T. Mahoney, C.K. Yao, and H.J. Bellen. 2009. Rab3 GTPase lands Bruchpilot. *Neuron.* 64:595–597. doi:10.1016/j.neuron.2009.11.029

Graf, E.R., R.W. Daniels, R.W. Burgess, T.L. Schwarz, and A. DiAntonio. 2009. Rab3 dynamically controls protein composition at active zones. *Neuron.* 64:663–677. doi:10.1016/j.neuron.2009.11.002

Hallam, S.J., A. Goncharov, J. McEwen, R. Baran, and Y. Jin. 2002. SYD-1, a presynaptic protein with PDZ, C2 and rhoGAP-like domains, specifies axon identity in *C. elegans*. *Nat. Neurosci.* 5:1137–1146. doi:10.1038/nn959

Jin, Y., and C.C. Garner. 2008. Molecular mechanisms of presynaptic differentiation. *Annu. Rev. Cell Dev. Biol.* 24:237–262. doi:10.1146/annurev.cellbio.23.090506.123417

Johnson, E.L. III, R.D. Fetter, and G.W. Davis. 2009. Negative regulation of active zone assembly by a newly identified SR protein kinase. *PLoS Biol.* 7:e1000193. doi:10.1371/journal.pbio.1000193

Kaufmann, N., J. DeProto, R. Ranjan, H. Wan, and D. Van Vactor. 2002. *Drosophila* liprin-alpha and the receptor phosphatase Dlar control synapse morphogenesis. *Neuron.* 34:27–38. doi:10.1016/S0896-6273(02)00643-8

Kittel, R.J., C. Wichmann, T.M. Rasse, W. Fouquet, M. Schmidt, A. Schmid, D.A. Wagh, C. Pawlu, R.R. Kellner, K.I. Willig, et al. 2006. Bruchpilot

promotes active zone assembly, Ca2+ channel clustering, and vesicle release. *Science.* 312:1051–1054. doi:10.1126/science.1126308

Leiss, F., E. Koper, I. Hein, W. Fouquet, J. Lindner, S. Sigrist, and G. Tavosanis. 2009. Characterization of dendritic spines in the *Drosophila* central nervous system. *Dev. Neurobiol.* 69:221–234. doi:10.1002/dneu.20699

Li, J., J. Ashley, V. Budnik, and M.A. Bhat. 2007. Crucial role of *Drosophila* neurexin in proper active zone apposition to postsynaptic densities, synaptic growth, and synaptic transmission. *Neuron.* 55:741–755. doi:10.1016/j.neuron.2007.08.002

Liebl, F.L., K. Chen, J. Karr, Q. Sheng, and D.E. Featherstone. 2005. Increased synaptic microtubules and altered synapse development in *Drosophila* sec8 mutants. *BMC Biol.* 3:27. doi:10.1186/1741-7007-3-27

Luo, L., T. Lee, L. Tsai, G. Tang, L.Y. Jan, and Y.N. Jan. 1997. Genghis Khan (Gek) as a putative effector for *Drosophila* Cdc42 and regulator of actin polymerization. *Proc. Natl. Acad. Sci. USA.* 94:12963–12968. doi:10.1073/pnas.94.24.12963

Mahr, A., and H. Aberle. 2006. The expression pattern of the *Drosophila* vesicular glutamate transporter: a marker protein for motoneurons and glutamatergic centers in the brain. *Gene Expr. Patterns.* 6:299–309. doi:10.1016/j.modgep.2005.07.006

Margeta, M.A., K. Shen, and B. Grill. 2008. Building a synapse: lessons on synaptic specificity and presynaptic assembly from the nematode *C. elegans*. *Curr. Opin. Neurobiol.* 18:69–76. doi:10.1016/j.conb.2008.04.003

Marrus, S.B., S.L. Portman, M.J. Allen, K.G. Moffat, and A. DiAntonio. 2004. Differential localization of glutamate receptor subunits at the *Drosophila* neuromuscular junction. *J. Neurosci.* 24:1406–1415. doi:10.1523/JNEUROSCI.1575-03.2004

Miller, K.E., J. DeProto, N. Kaufmann, B.N. Patel, A. Duckworth, and D. Van Vactor. 2005. Direct observation demonstrates that Liprin-alpha is required for trafficking of synaptic vesicles. *Curr. Biol.* 15:684–689. doi:10.1016/j.cub.2005.02.061

Nieratschker, V., A. Schubert, M. Jauch, N. Bock, D. Bucher, S. Dippacher, G. Krohne, E. Asan, S. Buchner, and E. Buchner. 2009. Bruchpilot in ribbon-like axonal agglomerates, behavioral defects, and early death in SRPK79D kinase mutants of *Drosophila*. *PLoS Genet.* 5:e1000700. doi:10.1371/journal.pgen.1000700

Owald, D., and S.J. Sigrist. 2009. Assembling the presynaptic active zone. *Curr. Opin. Neurobiol.* 19:311–318. doi:10.1016/j.conb.2009.03.003

Pack-Chung, E., P.T. Kurshan, D.K. Dickman, and T.L. Schwarz. 2007. A *Drosophila* kinesin required for synaptic bouton formation and synaptic vesicle transport. *Nat. Neurosci.* 10:980–989. doi:10.1038/nn1936

Parks, A.L., K.R. Cook, M. Belvin, N.A. Dompe, R. Fawcett, K. Huppert, L.R. Tan, C.G. Winter, K.P. Bogart, J.E. Deal, et al. 2004. Systematic generation of high-resolution deletion coverage of the *Drosophila* melanogaster genome. *Nat. Genet.* 36:288–292. doi:10.1038/ng1312

Patel, M.R., and K. Shen. 2009. RSY-1 is a local inhibitor of presynaptic assembly in *C. elegans*. *Science.* 323:1500–1503. doi:10.1126/science.1169025

Patel, M.R., E.K. Lehrman, V.Y. Poon, J.G. Crump, M. Zhen, C.I. Bargmann, and K. Shen. 2006. Hierarchical assembly of presynaptic components in defined *C. elegans* synapses. *Nat. Neurosci.* 9:1488–1498. doi:10.1038/nn1806

Petersen, S.A., R.D. Fetter, J.N. Noordermeer, C.S. Goodman, and A. DiAntonio. 1997. Genetic analysis of glutamate receptors in *Drosophila* reveals a retrograde signal regulating presynaptic transmitter release. *Neuron.* 19:1237–1248. doi:10.1016/S0896-6273(00)80415-8

Pilling, A.D., D. Horiuchi, C.M. Lively, and W.M. Saxton. 2006. Kinesin-1 and Dynein are the primary motors for fast transport of mitochondria in *Drosophila* motor axons. *Mol. Biol. Cell.* 17:2057–2068. doi:10.1091/mbc.E05-06-0526

Qin, G., T. Schwarz, R.J. Kittel, A. Schmid, T.M. Rasse, D. Kappei, E. Ponimaskin, M. Heckmann, and S.J. Sigrist. 2005. Four different subunits are essential for expressing the synaptic glutamate receptor at neuromuscular junctions of *Drosophila*. *J. Neurosci.* 25:3209–3218. doi:10.1523/JNEUROSCI.4194-04.2005

Raghu, S.V., M. Joesch, S.J. Sigrist, A. Borst, and D.F. Reiff. 2009. Synaptic organization of lobula plate tangential cells in *Drosophila*: Dalpha7 cholinergic receptors. *J. Neurogenet.* 23:200–209. doi:10.1080/01677060802471684

Rasse, T.M., W. Fouquet, A. Schmid, R.J. Kittel, S. Mertel, C.B. Sigrist, M. Schmidt, A. Guzman, C. Merino, G. Qin, et al. 2005. Glutamate receptor dynamics organizing synapse formation in vivo. *Nat. Neurosci.* 8:898–905.

Rostaing, P., E. Real, L. Siksou, J.P. Lechaire, T. Boudier, T.M. Boeckers, F. Gertler, E.D. Gundelfinger, A. Triller, and S. Marty. 2006. Analysis of synaptic ultrastructure without fixative using high-pressure freezing and tomography. *Eur. J. Neurosci.* 24:3463–3474. doi:10.1111/j.1460-9568.2006.05234.x

Schmid, A., G. Qin, C. Wichmann, R.J. Kittel, S. Mertel, W. Fouquet, M. Schmidt, M. Heckmann, and S.J. Sigrist. 2006. Non-NMDA-type glutamate receptors are essential for maturation but not for initial assembly of synapses at *Drosophila* neuromuscular junctions. *J. Neurosci.* 26:11267–11277. doi:10.1523/JNEUROSCI.2722-06.2006

Schmid, A., S. Hallermann, R.J. Kittel, O. Khorramshahi, A.M. Frölich, C. Quentin, T.M. Rasse, S. Mertel, M. Heckmann, and S.J. Sigrist. 2008. Activity-dependent site-specific changes of glutamate receptor composition in vivo. *Nat. Neurosci.* 11:659–666. doi:10.1038/nn.2122

Schoch, S., and E.D. Gundelfinger. 2006. Molecular organization of the presynaptic active zone. *Cell Tissue Res.* 326:379–391. doi:10.1007/s00441-006-0244-y

Shevchenko, A., M. Wilm, O. Vorm, and M. Mann. 1996. Mass spectrometric sequencing of proteins silver-stained polyacrylamide gels. *Anal. Chem.* 68:850–858. doi:10.1021/ac950914h

Shin, H., M. Wyszynski, K.H. Huh, J.G. Valtschanoff, J.R. Lee, J. Ko, M. Streuli, R.J. Weinberg, M. Sheng, and E. Kim. 2003. Association of the kinesin motor KIF1A with the multimodular protein liprin-alpha. *J. Biol. Chem.* 278:11393–11401. doi:10.1074/jbc.M211874200

Sigrist, S.J., D.F. Reiff, P.R. Thiel, J.R. Steinert, and C.M. Schuster. 2003. Experience-dependent strengthening of *Drosophila* neuromuscular junctions. *J. Neurosci.* 23:6546–6556.

Siksou, L., P. Rostaing, J.P. Lechaire, T. Boudier, T. Ohtsuka, A. Fejtová, H.T. Kao, P. Greengard, E.D. Gundelfinger, A. Triller, and S. Marty. 2007. Three-dimensional architecture of presynaptic terminal cytomatrix. *J. Neurosci.* 27:6868–6877. doi:10.1523/JNEUROSCI.1773-07.2007

Südhof, T.C. 2008. Neuroligins and neurexins link synaptic function to cognitive disease. *Nature.* 455:903–911. doi:10.1038/nature07456

van Roessel, P., D.A. Elliott, I.M. Robinson, A. Prokop, and A.H. Brand. 2004. Independent regulation of synaptic size and activity by the anaphase-promoting complex. *Cell.* 119:707–718. doi:10.1016/j.cell.2004.11.028

Wagh, D.A., T.M. Rasse, E. Asan, A. Hofbauer, I. Schwenkert, H. Dürrbeck, S. Buchner, M.C. Dabauvalle, M. Schmidt, G. Qin, et al. 2006. Bruchpilot, a protein with homology to ELKS/CAST, is required for structural integrity and function of synaptic active zones in *Drosophila*. *Neuron.* 49:833–844. doi:10.1016/j.neuron.2006.02.008

Wagner, O.I., A. Esposito, B. Köhler, C.W. Chen, C.P. Shen, G.H. Wu, E. Butkevich, S. Mandalapu, D. Wenzel, F.S. Wouters, and D.R. Klopfenstein. 2009. Synaptic scaffolding protein SYD-2 clusters and activates kinesin-3 UNC-104 in *C. elegans*. *Proc. Natl. Acad. Sci. USA.* 106:19605–19610. doi:10.1073/pnas.0902949106

Wairkar, Y.P., H. Toda, H. Mochizuki, K. Furukubo-Tokunaga, T. Tomoda, and A. Diantonio. 2009. Unc-51 controls active zone density and protein composition by downregulating ERK signaling. *J. Neurosci.* 29:517–528. doi:10.1523/JNEUROSCI.3848-08.2009

Wu, J.S., and L. Luo. 2006. A protocol for dissecting *Drosophila melanogaster* brains for live imaging or immunostaining. *Nat. Protoc.* 1:2110–2115. doi:10.1038/nprot.2006.336

Wyszynski, M., E. Kim, A.W. Dunah, M. Passafaro, J.G. Valtschanoff, C. Serra-Pagès, M. Streuli, R.J. Weinberg, and M. Sheng. 2002. Interaction between GRIP and liprin-alpha/SYD2 is required for AMPA receptor targeting. *Neuron.* 34:39–52. doi:10.1016/S0896-6273(02)00640-2